

OXIDIZED CARBON PARTICLES FROM STYRENE



A Thesis Submitted in Partial Fulfillment of the Requirements

for the Degree of Master of Science in Chemistry

Department of Chemistry

Faculty of Science

Chulalongkorn University

Academic Year 2018

Copyright of Chulalongkorn University

อนุภาคออกไซด์คาร์บอนจากสไตรีน



วิทยานิพนธ์นี้เป็นส่วนหนึ่งของการศึกษาตามหลักสูตรปริญญาวิทยาศาสตรมหาบัณฑิต

สาขาวิชาเคมี ภาควิชาเคมี

คณะวิทยาศาสตร์ จุฬาลงกรณ์มหาวิทยาลัย

ปีการศึกษา 2561

ลิขสิทธิ์ของจุฬาลงกรณ์มหาวิทยาลัย

| | |
|----------------|--|
| Thesis Title | OXIDIZED CARBON PARTICLES FROM STYRENE |
| By | Miss Titiporn Sansureerungsikul |
| Field of Study | Chemistry |
| Thesis Advisor | Professor Supason Wanichwecharungruang, Ph.D. |
| Co Advisor | Assistant Professor Thanakorn Wasanapiarnpong, Ph.D. |

Accepted by the Faculty of Science, Chulalongkorn University in Partial
Fulfillment of the Requirement for the Master of Science

..... Dean of the Faculty of Science
(Professor POLKIT SANGVANICH, Ph.D.)

THEESIS COMMITTEE

..... Chairman
(Associate Professor Vudhichai Parasuk, Ph.D.)

..... Advisor
(Professor Supason Wanichwecharungruang, Ph.D.)

..... Co-Advisor
(Assistant Professor Thanakorn Wasanapiarnpong, Ph.D.)

..... Examiner
(Numpon Insin, Ph.D.)

..... External Examiner
(Assistant Professor Thitinun Karpkird, Ph.D.)

ฐิติพร แสนสุรีย์รังสิกุล : อนุภาคออกซิไดส์คาร์บอนจากสไตรีน. (OXIDIZED

CARBON PARTICLES FROM STYRENE) อ.ที่ปรึกษาหลัก : ศ. ดร.ศุภศร วณิชเวชา

รุ่งเรือง, อ.ที่ปรึกษาร่วม : ผศ. ดร.ธนากร วาสนาเพียรพงศ์

เป็นการสังเคราะห์อนุภาคออกซิไดส์คาร์บอนรูปทรงกลมขนาดต่างๆ โดยใช้สไตรีนมอนอเมอร์จากการผ่านกระบวนการ 4 ขั้นตอนคือ การเตรียมอนุภาคพอลิสไตรีนขนาดต่างๆจากการปรับความเข้มข้นของมอนอเมอร์ สารลดแรงตึงผิว และอุณหภูมิของปฏิกิริยา และนำอนุภาคพอลิสไตรีนที่ได้มาทำ hypercrosslink ด้วยปฏิกิริยา Friedel-Craft alkylation reaction จากนั้นนำอนุภาคที่ได้จากการ hypercrosslink มาเผาภายใต้บรรยากาศของแก๊สไนโตรเจนเพื่อให้ได้อนุภาคคาร์บอนรูปทรงกลมขนาดต่างๆ จากนั้นเลือกอนุภาคคาร์บอนแต่ละขนาดมาทำปฏิกิริยาออกซิเดชันด้วยโพแทสเซียมเปอร์แมงกาเนต กรดซัลฟิวริกเข้มข้น และโซเดียมไนเตรตเพื่อให้ได้อนุภาคออกซิไดส์คาร์บอนรูปทรงกลมขนาด ๓๓ ต่าง โดยได้ทำการเปรียบเทียบความสามารถในเกาะเหนียวทำให้เกิดรูพรุนไลโปโซมของอนุภาคออกซิไดส์คาร์บอนขนาดต่าง ๆ จากการสังเกตการรั่วของน้ำตาลของไลโปโซม พบว่าอนุภาคออกซิไดส์คาร์บอนรูปทรงกลมขนาดประมาณ 140 นาโนเมตรสามารถทำให้เกิดรูพรุนไลโปโซมได้มากที่สุด

จุฬาลงกรณ์มหาวิทยาลัย
CHULALONGKORN UNIVERSITY

สาขาวิชา เคมี

ลายมือชื่อนิสิต

.....

ปี 2561

ลายมือชื่อ อ.ที่ปรึกษาหลัก

การศึกษา

.....

ลายมือชื่อ อ.ที่ปรึกษาร่วม

.....

5871944223 : MAJOR CHEMISTRY

KEYWORD: oxidized carbon nanospheres/lipid bilayer membrane/size

Titiporn Sansureerungsikul : OXIDIZED CARBON PARTICLES FROM STYRENE. Advisor: Prof. Supason Wanichwecharungruang, Ph.D.,Asst. Prof. Thanakorn Wasanapiarnpong, Ph.D.

It has been reported the spherical shape of oxidized carbon nanoparticulates shows higher ability to penetrate phospholipid bilayer membrane than tubular and sheet shapes. However, the effect of the particle size on this membrane penetration ability have never been investigated. In this work, we synthesized various sizes of oxidized carbon spheres through a four steps process. Firstly, we adjusted the surfactants and styrene concentrations to prepare polystyrene of various sizes. Then, the polystyrene particles of selected sizes were hypercrosslinked via Friedel-Craft alkylation reaction. After that, hypercrosslinked polystyreneparticles were pyrolyzed under N_2 atmosphere to obtain carbon nanospheres of various sizes. The obtained carbon particles of selected sizes were then oxidized using the mixture of $KMnO_4$, H_2SO_4 and $NaNO_3$. Ability of the resulted oxidized carbon particles to induce membrane leakage of cell-size liposome was then investigated by sugar leak experiment. The results show that oxidized carbon particle with the size of around 140 nm can most effectively induce membrane leakage.

Field of Study: Chemistry

Student's Signature

.....

Academic Year: 2018

Advisor's Signature

.....

Co-advisor's Signature

.....

ACKNOWLEDGEMENTS

Firstly, I would like to express my sincere gratitude to my advisor Prof. Supason Wanichwecharungruang and my co-advisor Asst. Prof. Thanakorn Wasanapiarnpong for the continuous support of my Master degree study and related research, for their patience, motivation, and immense knowledge. Their guidance helped me in all the time of research and writing of this thesis.

I am sincerely grateful to the members of the thesis committee, Assoc. Prof. Vudhichai Parasuk, Dr. Numpon Insin, Asst. Prof. Thitinun Karpkird for their valuable comments and suggestion.

I would like to acknowledge the members of the SW research group on fourteenth floor, Mahamakut building for their companionship and friendship. And I would like to thank some special lovely partners, Eakkaphon Rattanangkool, Pornpan Nutthawut, Parichat Tawornchat and Vasin Thummasorn and for their suggestion and friendship.

Nobody has been more important to me in the pursuit of this project than the members of my family. I would like to thank and take this opportunity to express my sincere appreciation to my parents for their encouragement, activation, and support throughout the entire research study. This accomplishment would not have been possible without them.

จุฬาลงกรณ์มหาวิทยาลัย
CHULALONGKORN UNIVERSITY

Titiporn Sansureerungsikul

TABLE OF CONTENTS

| | Page |
|--|------|
| | iii |
| ABSTRACT (THAI)..... | iii |
| | iv |
| ABSTRACT (ENGLISH) | iv |
| ACKNOWLEDGEMENTS..... | v |
| TABLE OF CONTENTS..... | vi |
| LIST OF TABLES..... | I |
| LIST OF FIGURES | J |
| CHAPTER I INTRODUCTION | 1 |
| 1.1 INTRODUCTION | 1 |
| 1.2 LITERATURE REVIEWS..... | 1 |
| 1.2.1 Delivery of bio-macromolecules into the cell | 1 |
| 1.2.1.1 Cationic liposome | 3 |
| 1.2.1.2 Electroporation..... | 3 |
| 1.2.1.3 Nonlipid vesicular particulate system..... | 4 |
| 1.2.2 Carrier and uptake ability | 5 |
| 1.2.2.1 Shape | 5 |
| 1.2.2.2 Surface charge | 6 |
| 1.2.2.3 Size..... | 6 |
| 1.2.3 Oxidized carbon nanospheres..... | 7 |
| 1.2.4 Carbon nanospheres..... | 7 |

| | |
|---|----|
| 1.2.4.2 Carbon nanospheres from pyrolytic carbonization | 8 |
| 1.2.5 Polystyrene particles | 9 |
| 1.2.6 Liposome | 10 |
| 1.3 Objective | 12 |
| CHAPTER II EXPERIMENTAL..... | 13 |
| 2.1 Materials and chemicals | 13 |
| 2.2 Synthesis and characterization of polystyrene particles (PSs) | 14 |
| 2.3 Synthesis and characterization of hyper crosslink-polystyrene particles (HC-PSs) | 15 |
| 2.4 Synthesis and characterization of carbon nanosphere particle (C) | 16 |
| 2.5 Synthesis and characterization of oxidized carbon particles (OPs) | 16 |
| 2.6 Effect of particles size of oxidized carbon particles on their ability to induce a leakage on lipid bilayer membrane | 17 |
| CHAPTER III RESULTS AND DISCUSSIONS..... | 19 |
| 3.1 Synthesis and characterization of polystyrene particles (PSs) | 19 |
| 3.2 Synthesis and characterization of the hyper crosslink-polystyrene particles (HC- PSs)..... | 24 |
| 3.3 Synthesis and characterization of carbon nanosphere particles (C)..... | 29 |
| 3.4 Synthesis and characterization of oxidized carbon particles (OPs) | 38 |
| 3.4.1 Oxidized carbon particles from C1 | 38 |
| 3.4.2 Oxidized carbon particles from C3..... | 40 |
| 3.4.3 Oxidized carbon particles from C7 | 41 |
| 3.5 Effect of particles size of oxidized carbon particles on their ability to induce a leakage on lipid bilayer membrane..... | 47 |

| | |
|----------------------------|----|
| CHAPER IV CONCLUSION | 51 |
| REFERENCES..... | 53 |
| VITA | 57 |



LIST OF TABLES

| | | |
|------------|---|----|
| Table 2. 1 | The amount of reagents for the preparation of polystyrene particles..... | 14 |
| Table 2. 2 | The specific experiment time for hyper crosslink-polystyrene reaction. | 15 |
| Table 2. 3 | The amount of reagent for the oxidation reaction of carbon particles..... | 17 |
| Table 3. 1 | Size of PSs were prepared under different conditions | 20 |
| Table 3. 2 | Size of HC-PSs prepared from PSs as starting material under a specific time. | 25 |
| Table 3. 3 | Size of all products prepared by pyrolytic carbonization under different time conditions. | 30 |
| Table 3. 4 | The amount of reagent for the oxidation reaction of C1 (carbon particles).... | 38 |
| Table 3. 5 | The amount of reagent for the oxidation reaction of C3 and C7 (carbon particles)..... | 40 |
| Table 3. 6 | The sizes and zeta potentials of the three selected oxidized carbon particles | 41 |
| Table 4. 1 | Summary of particle size in each step of oxidized carbon nanosphere preparation and their ability to induce a leakage on lipid bilayer membrane..... | 52 |

LIST OF FIGURES

| | |
|--|----|
| Figure 1. 1 Schematic representation of the ssDNA assisted CPP–DNA conjugation strategy for constructing covalent CPP–DNA fluorescent probes [3]..... | 3 |
| Figure 1. 2 Electroporation phenomenon. Electric field disrupts cell membrane allowing molecules poration [6]..... | 4 |
| Figure 1. 3 Illustration summarizing different NPs and characteristics important for their properties [9]..... | 5 |
| Figure 1. 4 Schematic illustration size-dependence of particle association with lipid bilayer membrane in the different fluidity of lipid [13] | 7 |
| Figure 1. 5 Diagram for preparation of monodisperse microporous polymeric and carbonaceous nanospheres [20]..... | 8 |
| Figure 1. 6 The mechanism of free radical polymerization of styrene monomer..... | 9 |
| Figure 1. 7 (a) The structure of one POPC (1-palmitoyl-2-oleoyl-sn-glycero-3-phosphocholine) lipid molecule, showing the hydrophilic head and hydrophobic tail. POPC is a naturally-occurring lipid and is commonly used in the production of synthetic liposomes. (b) The heads and tails of the lipid interact to self-assemble into a membrane structure, and (c) a lipid vesicle [24] | 11 |
| Figure 1. 8 The common vesicle size and lamellarity classification system often used with liposome. Small unilamellar vesicles (SUV) are less than 100 nm in diameter; large unilamellar vesicles (LUV) are between 100 and 1000 nm, and giant unilamellar vesicles (GUV) are larger than 1 micron. Multilamellar vesicles have many membrane layers, and multivesicular vesicles encapsulate smaller vesicles [24] | 11 |
| Figure 2. 1 The layer of the lipid film, chamber, and ITO-glass for liposome preparation by electroformation method | 17 |

| | |
|--|----|
| Figure 3. 1 Morphology of all PSs were prepared under different conditions | 19 |
| Figure 3. 2 The mechanism of emulsion polymerization (a) and polymerization mechanism of styrene and DVB monomer (b)..... | 22 |
| Figure 3. 3 The Fourier transform infrared (FT-IR) spectra of all PSs | 23 |
| Figure 3. 4 The Thermogravimetric analysis of all PSs | 23 |
| Figure 3. 5 Morphology characterization of HC-PSs prepared under different conditions | 25 |
| Figure 3. 6 The Fourier transform infrared (FT-IR) spectra of all HC-PSs | 26 |
| Figure 3. 7 The Thermogravimetric analysis of all HC-PSs..... | 27 |
| Figure 3. 8 The mechanism of hyper crosslink-polystyrene particles via Friedel-Craft alkylation..... | 28 |
| Figure 3. 9 Morphology characterization of all products prepared from pyrolytic carbonization..... | 29 |
| Figure 3. 10 The Thermogravimetric analysis of all products prepared from pyrolytic carbonization..... | 30 |
| Figure 3. 11 The FT-IR spectra of all products prepared from pyrolytic carbonization .. | 31 |
| Figure 3. 12 The Raman spectrums of all products prepared from pyrolytic carbonization..... | 32 |
| Figure 3. 13 The XPS spectrum of all carbon samples, survey scan spectra (a) and deconvolutes C1s, O1s and N1s fitting spectra (b and c) | 36 |
| Figure 3. 14 The SEM images of oxidized carbon particles which are prepared from C1 in different conditions | 39 |
| Figure 3. 15 The SEM image of the OP3.1 (a) and OP7.1 (b) | 40 |
| Figure 3. 16 Water dispersibility of carbon particles (top) and oxidized carbon particles (bottom) | 42 |

| | |
|--|----|
| Figure 3. 17 The FT-IR spectra of all oxidized carbon particles | 43 |
| Figure 3. 18 The Raman spectra of oxidized carbon particles (red) comparing with their parent carbon particles (blue) | 44 |
| Figure 3. 19 C1s, O1s, and N1s of XPS spectra of OP1.5, OP3.1, and OP7.1 | 45 |
| Figure 3. 20 A shortened scheme of the proposed mechanism of oxidation of carbon particles | 47 |
| Figure 3. 21 The untreated liposome (a) and liposome after glucose adding (b)..... | 48 |
| Figure 3. 22 Phase contrast image of liposome after being incubated with oxidized carbon particles for 30, 60, 120 and 240 min..... | 49 |
| Figure 3. 23 The percentage of phase contrast changed of liposome after incubated with oxidized carbon particles for 30, 60, 120 and 240 min. | 50 |
| Figure 3. 1 Morphology of all PSs were prepared under different conditions | 19 |
| Figure 3. 2 The mechanism of emulsion polymerization (a) and polymerization mechanism of styrene and DVB monomer (b)..... | 22 |
| Figure 3. 3 The Fourier transform infrared (FT-IR) spectra of all PSs | 23 |
| Figure 3. 4 The Thermogravimetric analysis of all PSs | 23 |
| Figure 3. 5 Morphology characterization of HC-PSs prepared under different conditions | 25 |
| Figure 3. 6 The Fourier transform infrared (FT-IR) spectra of all HC-PSs..... | 26 |
| Figure 3. 7 The Thermogravimetric analysis of all HC-PSs..... | 27 |
| Figure 3. 8 The mechanism of hyper crosslink-polystyrene particles via Friedel-Craft alkylation..... | 28 |
| Figure 3. 9 Morphology characterization of all products prepared from pyrolytic carbonization..... | 29 |

| | |
|---|----|
| Figure 3. 10 The Thermogravimetric analysis of all products prepared from pyrolytic carbonization..... | 30 |
| Figure 3. 11 The FT-IR spectra of all products prepared from pyrolytic carbonization .. | 31 |
| Figure 3. 12 The Raman spectrums of all products prepared from pyrolytic carbonization..... | 32 |
| Figure 3. 13 The XPS spectrum of all carbon samples, survey scan spectra (a) and deconvolutes C1s, O1s and N1s fitting spectra (b and c) | 36 |
| Figure 3. 14 The SEM images of oxidized carbon particles which are prepared from C1 in different conditions | 39 |
| Figure 3. 15 The SEM image of the OP3.1 (a) and OP7.1 (b) | 40 |
| Figure 3. 16 Water dispersibility of carbon particles (top) and oxidized carbon particles (bottom) | 42 |
| Figure 3. 17 The FT-IR spectra of all oxidized carbon particles | 43 |
| Figure 3. 18 The Raman spectra of oxidized carbon particles (red) comparing with their parent carbon particles (blue) | 44 |
| Figure 3. 19 C1s, O1s, and N1s of XPS spectra of OP1.5, OP3.1, and OP7.1 | 45 |
| Figure 3. 20 A shortened scheme of the proposed mechanism of oxidation of carbon particles | 47 |
| Figure 3. 21 The untreated liposome (a) and liposome after glucose adding (b)..... | 48 |
| Figure 3. 22 Phase contrast image of liposome after being incubated with oxidized carbon particles for 30, 60, 120 and 240 min..... | 49 |
| Figure 3. 23 The percentage of phase contrast changed of liposome after incubated with oxidized carbon particles for 30, 60, 120 and 240 min. | 50 |
| Figure 4. 1 Illusion for preparation of various sized of oxidized carbon nanosphere and study their ability to induce a leakage on lipid bilayer membrane | 51 |



จุฬาลงกรณ์มหาวิทยาลัย
CHULALONGKORN UNIVERSITY

CHAPTER I

INTRODUCTION

1.1 INTRODUCTION

Various scientific investigation and therapeutic works require the transport of biomacromolecules such as antisense oligonucleotide, siRNA and peptide into cells. There are many techniques to deliver macromolecules into the cell such as cell-penetrating peptides (CPPs), cationic lipid, nonlipid vesicular particulate system, and electroporation. The purpose of these techniques is to improve efficiency of macromolecules delivery. Other advantages associated with the use of these delivering system are improving ability of vaccine, drug solubility, organelle targeting and prolongation of drug lifetime in the circulation system. However, lysosome trapping, low transfection efficiency, toxicity, and limited loading are disadvantages of these methods¹⁻⁸. Oxidized carbon nanospheres (OCNs) prepared by oxidation of graphite under strong acid and strong sonication condition, these materials can facilitate the penetration of peptide nucleic acid across a cell membrane without being trapped in lysosome¹⁴⁻¹⁵. It has been reported that the OCNs exhibit higher penetration ability to phospholipid bilayer membrane than tubular and sheet shape¹⁶. However, the effect of the size of the OCNs has never been investigated. Therefore, this research focuses on the effect of size of the oxidized carbon particles on the induction of membrane leakage of the cell-sized liposomes.

1.2 LITERATURE REVIEWS

1.2.1 Delivery of bio-macromolecules into the cell

Biomacromolecules including antisense oligonucleotide, small interfering RNA (siRNAs), and peptide have many desirable therapeutic features that provide unique opportunities to design precision medicine therapeutics to treat human disease. However, macromolecules cannot pass through the cell membrane and enter cells due

to their sizes. The penetration of biomacromolecules is enhanced by some techniques of the delivery system as shown below.

1.2.1.1 Cell penetrating peptide

Cell-penetrating peptides or CPPs is the relatively short cationic and/or amphipathic peptides. CPPs have received great attention as efficient cellular delivery vectors due to their intrinsic ability to get into cells and mediate cellular uptake of a wide range of macromolecular cargo such as plasmid DNA (pDNA), siRNAs, drugs, and nanoparticulate pharmaceutical carriers ¹⁻².

Chen and co-workers demonstrated the electrostatic interactions between CPPs and single-stranded DNA (ssDNA). The results showed the stronger CPPs-ssDNA interaction than those between CPPs and double-stranded DNA (dsDNA). In addition, they developed the ssDNA protected CPP-DNA fluorescent probe which allowed noninvasive and efficient cellular uptake and rapid imaging of target nucleases in living cells. The probe is highly sensitive and selective. This work represents the first example of using CPPs-DNA conjugation for DNA fluorescent probes delivery. The probe can be used as *in situ* imaging of nuclease within the cell. However, the linear working range of the conjugated probe was from 40 to 500 U/L ³.

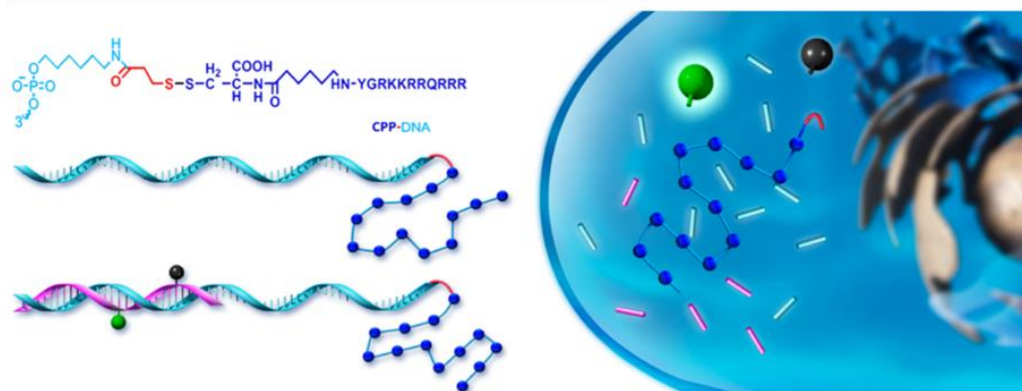


Figure 1. 1 Schematic representation of the ssDNA assisted CPP-DNA conjugation strategy for constructing covalent CPP-DNA fluorescent probes ³

1.2.1.2 Cationic liposome

Cationic liposome composes of positively charged amphipathic molecules which self-assemble in water to form vesicles. The positive charged amphipathic molecules including cationic polar head, hydrophobic chain, and a linker. It has been reported that the cationic liposome efficiently interacts with a negative charge of biomacromolecules (such as siRNA or DNA) by electrostatic force. This method is fast, easy and effective to deliver macromolecules across the cell membrane. However, their method is concerned about stability of liposome ⁴.

1.2.1.3 Electroporation

Electroporation technique uses the short high-voltage pulses to generate the barrier of the cell membrane. The local transient and reversible breakdown of the membrane can be induced by applying the external electric field to cell. The variety of different molecules including oligonucleotide molecules can pass through the transient pore. However, cells are probably damaged by the external electric field ⁵.

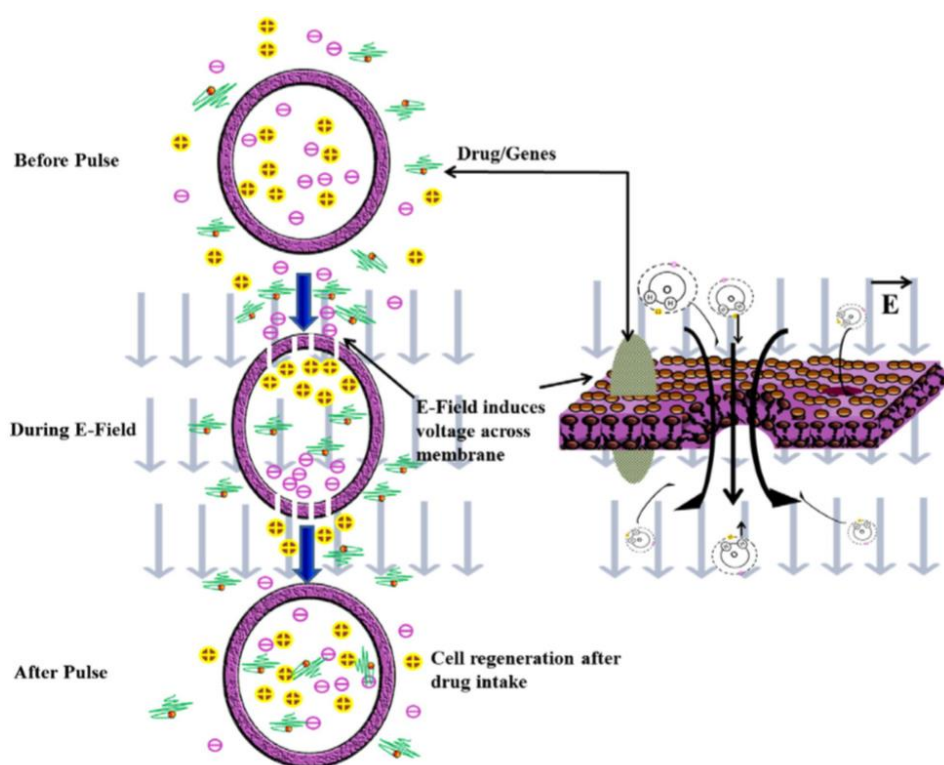


Figure 1. 2 Electroporation phenomenon. Electric field disrupts cell membrane allowing molecules poration ⁶

1.2.1.4 Nonlipid vesicular particulate system

It has been reported that the drug delivery system has been developed using nanotechnology to enhance important characteristics of a drug such as bioavailability, drug solubility and minimized side effect. Polymeric nanoparticle, nanocrystal and nanospheres are the some types of nanotechnology for drug delivery [7]. However, nonlipid vesicular particulate system is mostly entered the cell by endocytosis pathway ⁷. By this pathway, drug or interested molecules and nanoparticle are wrapped by cell-membrane to form an endocytic vesicle. The endocytic vesicle is transported to the cytosol of the cell and fused with a lysosome. Then, the cargo is destroyed by lysosome or released into the cytosol ⁸.

1.2.2 Carrier and uptake ability

Nanomaterial has various factor of cellular penetration such as surface chemistry, composition, shape, size and target element of nanoparticle as shown in Figure 1.3.

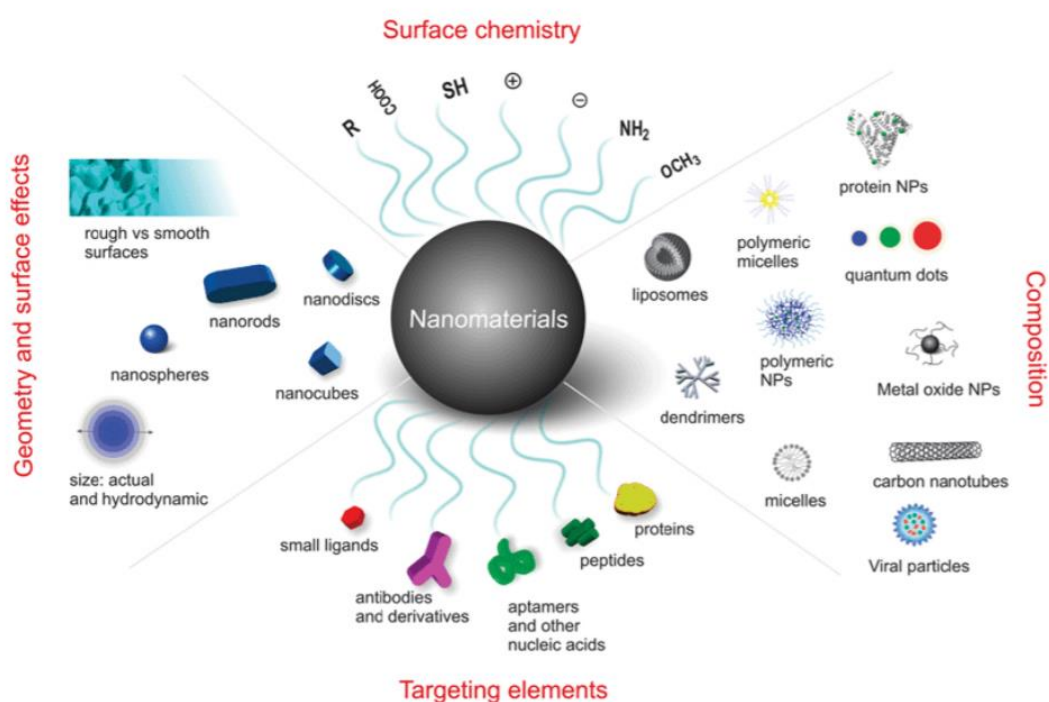


Figure 1. 3 Illustration summarizing different NPs and characteristics important for their properties ⁹

1.2.2.1 Shape

Many previous researches have been reported that the interaction between cell membrane and nanoparticles is significantly affected by the shape of nanoparticles.

Tree-Udom and co-worker prepared Lanthanide-doped NaYF_4 nanoparticles with three different shapes were a sphere, elongated sphere, and

hexagonal prism. The results showed that the elongated spherical particles have higher cellular internalization than the other shapes ¹⁰

1.2.2.2 Surface charge

The surface charge of a particle is a key parameter determining nanoparticles which their interaction with cell membrane and adsorption property of protein on nanoparticles ¹¹.

Mullen and co-worker prepared positive and negative charge of gold nanoparticles to study charge-dependent interactions of gold nanoparticles with biological media and nanoparticle uptake by cells. The result revealed that the positively charged gold nanoparticles are incorporated faster than the negative charge ones in several cell lines ¹².

1.2.2.3 Size

The size of nanoparticles controls the interaction of particles with the cell membrane and ultimately their intracellular uptake.

Hamada and co-worker reported that the size of particle intensely affected the selective association with lipid bilayer membrane. They studied the various sizes of polystyrene particle with two types of lipid membrane (high (L_d) and low (L_o) fluidity). The result showed that the small size of particle (200nm) are preferred to interact with the low fluidity membrane. While the size of particle higher than 200 nm are favor to interact with the high fluidity ¹³.

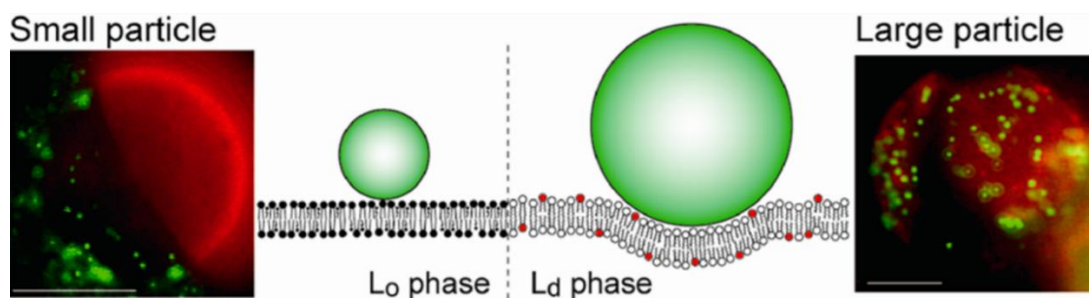


Figure 1. 4 Schematic illustration size-dependence of particle association with lipid bilayer membrane in the different fluidity of lipid ¹³

1.2.3 Oxidized carbon nanospheres

Arayachukeat and co-worker successfully synthesized the oxidized carbon nanospheres (OCSs) via the oxidation of graphite. The average of particles size is around 130 nm. OCSs can deliver small/macromolecules into the cell by endocytosis with endosomal leakage ¹⁴⁻¹⁵. Subsequent, Seemork and co-worker studied the effect of the shape of oxidized carbon particles on their ability to penetrate the phospholipid bilayer membrane. The results indicated that the OCSs have higher ability to penetrate phospholipid bilayer membrane than the tubular and sheet shapes ¹⁶. However, the oxidized carbon nanospheres which are prepared from graphite were limited at 8% yield. Therefore, Amornwachirabodee and co-worker synthesized oxidized carbon nanospheres via commercially available carbon black instead of graphite. The results showed that OCSs which are prepared from carbon black has 18% yield. These OCSs still has ability to penetrate phospholipid bilayer membrane to induce phospholipid bilayer membrane leakages on cell-sized liposome and real cells ¹⁷.

1.2.4 Carbon nanospheres

The oxidized carbon nanospheres could be prepared from the oxidation of spherical-shaped carbon materials. Many previous researches have been reported that carbon nanosphere can be prepared from various techniques.

1.2.4.1 Carbon nanosphere from the petroleum industries

Carbon black is a material produced by the incomplete combustion of heavy petroleum product such as coal, tar or ethylene cracking tar. Certainly, there are many sizes of carbon black and they are used in tires, plastic, and paints. The size range of carbon black is around 25-350 nm ¹⁸.

1.2.4.2 Carbon nanospheres from pyrolytic carbonization

Carbonization is the pyrolytic process that converts organic substances to pure carbon or carbon-containing residues. The synthetic carbonization strategies towards carbon nanoparticles involve pyrolysis of organic precursor under inert atmospheres and chemical vapor deposition technique ¹⁹.

Ouyang and co-worker successfully synthesized monodisperse carbon nanoparticles with a diameter below 500 nm. In their work, they prepared carbon nanospheres via 3 step process as shown in Figure 1.5. Firstly, the various size of polystyrene particles (PSs) was prepared by emulsion polymerization of styrene and divinylbenzene monomer. To control the size of PSs, the concentration of surfactants was adjusted. The result showed the particle size of PSs is increased when the concentration of surfactant was increased. After that, PSs was hypercrosslinked via Friedel-Crafts reaction. Lastly, hypercrosslinked particles were carbonized to pyrolyzed monodisperse carbon nanospheres. ²⁰.

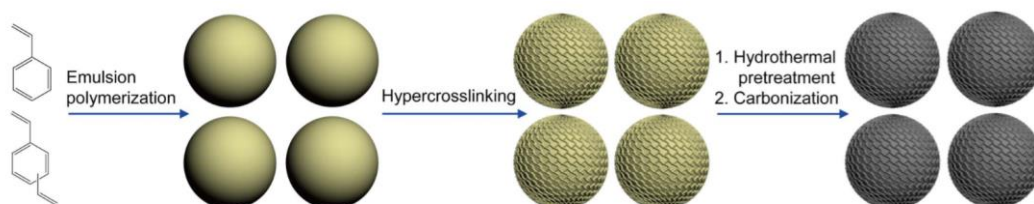


Figure 1. 5 Diagram for preparation of monodisperse microporous polymeric and carbonaceous nanospheres ²⁰

Lee and co-worker prepared monodispersed N-doped carbon nanospheres by pyrolytic carbonization of polymerized polystyrene in the presence of nitrogen-enrich molecules, melamine (1,3,5-Triazine-2,4,6-triamine). The diameter of these carbon nanospheres was around 300 nm. In their work, they used carbon nanospheres for supercapacitor application ²¹.

1.2.5 Polystyrene particles

According to carbon nanosphere can be prepared by pyrolytic carbonization of polystyrene particles (PSs). Many previous researches successfully control the size of polystyrene particle.

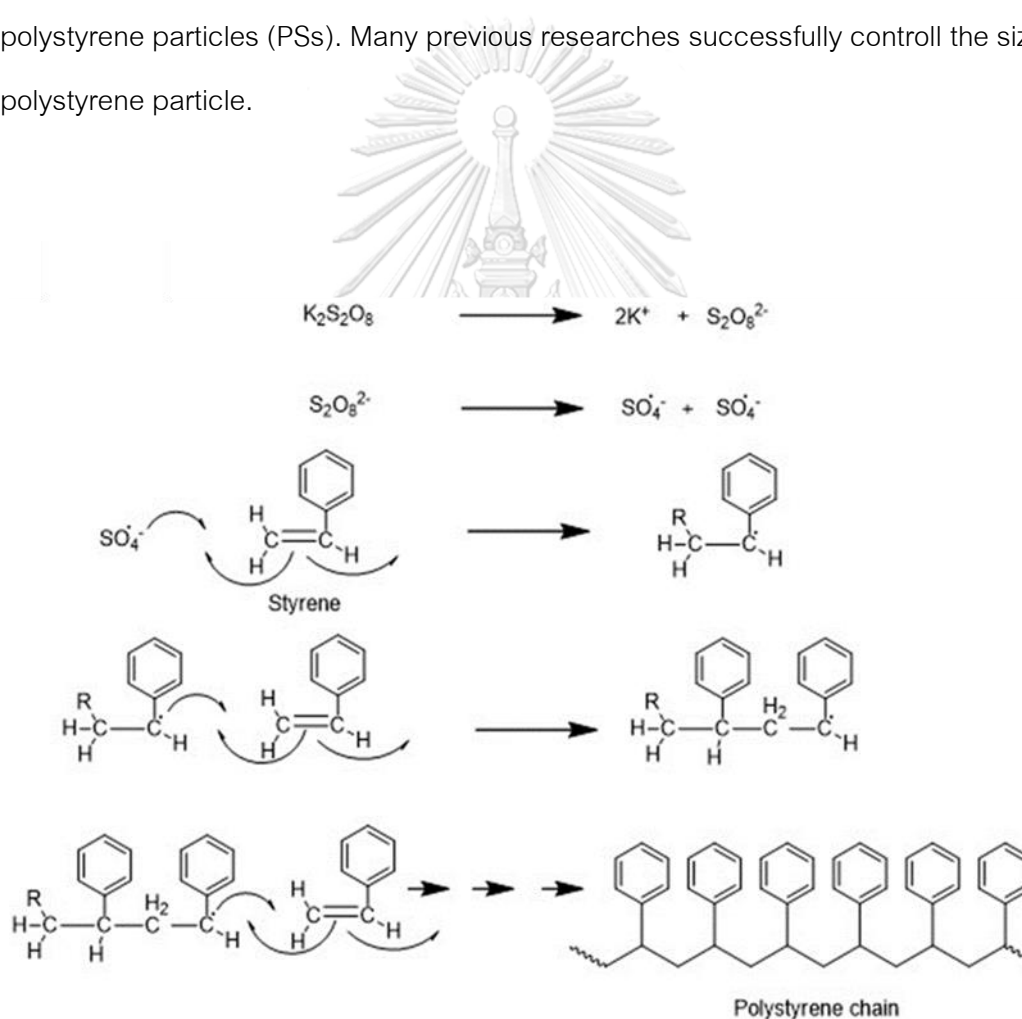


Figure 1. 6 The mechanism of free radical polymerization of styrene monomer

Jinhua and co-worker synthesized microspheres of PSs by dispersion polymerization in the mixed solvent between ethanol and water. In their work, they used styrene as a monomer, azobisisobutyronitrile (AIBN) as an initiator and polyvinylpyrrolidone (PVP) as a stabilizer. The result showed that the particle size of PSs is increase with decreasing of ethanol content. However, the monodisperse PSs were prepared by using pure solvent (water or ethanol). PSs prepared in mixed solvent gave polydisperse of PSs. The size of PSs which were prepared from this technique is around 0.3-5 micrometer²².

Shim and co-worker prepared micro-sized monodisperse crosslinked polystyrene bead by multistage polymerization in the absence of surfactant. This result exhibited the particles size is increase with the increasing of concentrations of initiator and monomer content. Their work also studied the effect of temperature on particles size. The results indicated that at low temperature of reaction (60°C), the bigger particles are obtained. While, at high temperature of reaction (80°C), the bigger particles were obtained²³.

1.2.6 Liposome

A liposome is a spherical lipid bilayer vesicle, which forms an internal cavity capable of carrying aqueous solutions. A lipid bilayer is composed of two sheets of tightly arranged phospholipids. These molecules have a hydrophobic tail and a hydrophilic head region such as POPC (1-palmitoyl-2-oleoyl-sn-glycero-3-phosphocholine) lipid molecule (shown in **Figure 1.7**). When two single membranes come together, the hydrophobic tails attract toward each other, while the heads of both membranes are attracted to the surrounding water. This forms a double layer of phospholipid molecules, which exclude the internal solution from the outside.

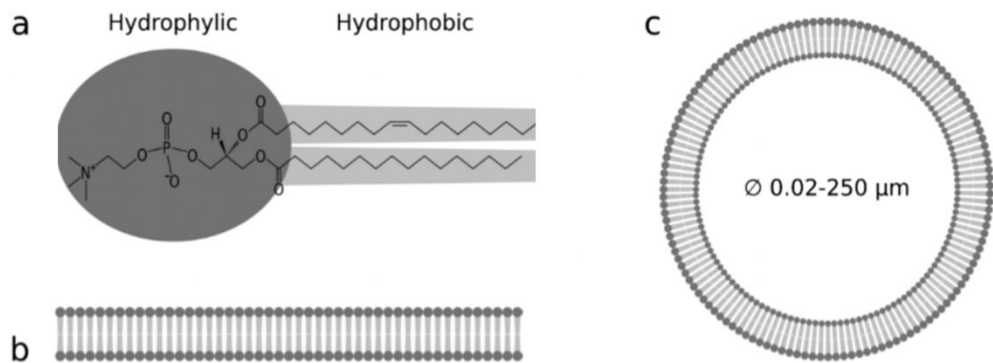


Figure 1. 7 (a) The structure of one POPC (1-palmitoyl-2-oleoyl-sn-glycero-3-phosphocholine) lipid molecule, showing the hydrophilic head and hydrophobic tail. POPC is a naturally-occurring lipid and is commonly used in the production of synthetic liposomes. (b) The heads and tails of the lipid interact to self-assemble into a membrane structure, and (c) a lipid vesicle ²⁴

Liposomes are frequently classified based on their size, a number of bilayer and phospholipid charge.

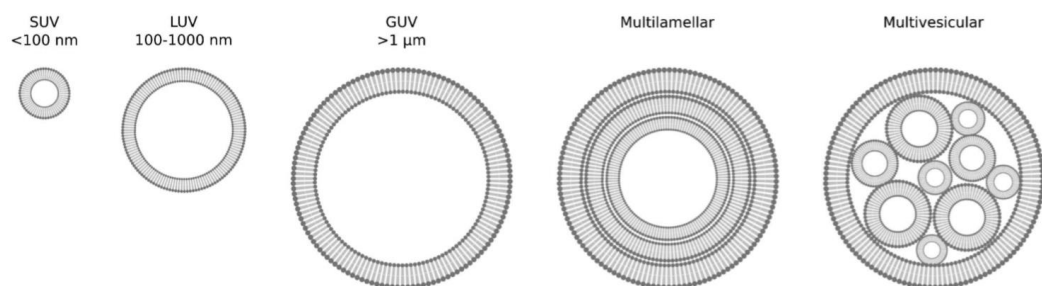


Figure 1. 8 The common vesicle size and lamellarity classification system often used with liposome. Small unilamellar vesicles (SUV) are less than 100 nm in diameter; large unilamellar vesicles (LUV) are between 100 and 1000 nm, and giant unilamellar vesicles (GUV) are larger than 1 micron. Multilamellar vesicles have many membrane layers, and multivesicular vesicles encapsulate smaller vesicles ²⁴

Giant unilamellar vesicles (GUVs) are well-established model systems for studying membrane structure and dynamics because their size is easy to observe. GUVs are prepared by hydration or electroformation methods. The hydration method contains deposition of phospholipids, from a solution in an organic solvent such as chloroform or ethanol, onto a substrate. The film consisting of stacked phospholipid bilayers is subsequently hydrated over a couple of days in the absence of hydrodynamic flow to obtain an aqueous suspension of GUVs²⁵. Electroformation method, the phospholipid film is deposited on electrodes and subsequently hydrated for a couple of hours in the presence of an electric field. However, GUVs are formed by the application of both alternating and direct current, DC fields are not preferred as they lead to bubbling due to electrolysis of water. It has been reported that 80% often electroformed vesicle population is unilamellar²⁵. Moreover, Lee and co-worker showed that the liposome were prepared by electroformation were strong enough to survive electroporation²⁶.

1.3 Objective

As mentioned above the information on the interesting ability to penetrate phospholipid bilayer membrane of oxidized carbon nanospheres (OCNs). However, the effect of size of the OCNs has never been investigated. Therefore, this research focused on the synthesis of the various sizes of oxidized carbon particles. The effect of size of oxidized carbon particles on the induction of membrane leakage of the cell-sized liposomes will be studied by sugar leak experiment.

CHAPTER II

EXPERIMENTAL

2.1 Materials and chemicals

Styrene monomer and dialysis cellulose membrane (MWCO= 12-14 kDa) were purchased from Sigma Aldrich (St. Louis, USA). Aluminium trichloride, potassium persulfate, divinylbenzene, 37% hydrochloric acid and 30% hydrogen peroxide solution were purchased from Merck KGaA (Darmstadt, Germany). Sodium dodecylbenzenesulfonate was purchased from Union Chemical 1986 (Bangkok, Thailand). Potassium permanganate, sodium nitrate, and crucible were purchased from the Office of the Welfare Promotion Commission for Teachers and Education Personnel (Bangkok, Thailand). Melamine monomer was purchased from TCI (Tokyo, Japan). 1,2-Dioleoyl-sn-glycero-3-phosphocholine (DOPC) was purchased from Avanti Polar Lipid (Alabama, USA). Chloroform, acetone, and ethanol were purchased from RCI Labscan (Bangkok, Thailand). All chemicals used were analytical grade and were used without further purification.

Freeze-drying was carried out by Freeze-dry/Shell Freeze System Model 7753501 (Labconco Corporation, Kansas, MI, USA). Functional groups on the particle surface were evaluated by AXIS-ULTRA DLD XSAM800 type x-ray photoelectron spectrometer (Shimadzu/Kratos), ATR-FTIR (Nicolet 6700, Thermo Electron Corporation, Madison, WI, USA) and DXR Raman microscope [(Thermo Electron Corporation, Madison, WI, USA) with a 10X objective and 5mW diode laser ($\lambda = 780$ nm) excitation source]. Scanning electron microscopic image of particles was obtained by JSM-7610 scanning electron microscope (JEOL, Tokyo, Japan). Zeta potential was evaluated by dynamic light scattering (DLS) with Zetasizer nano series instrument (Zs, Malvern Instruments, United Kingdom). Thermal analysis of particles was obtained by thermogravimetric analysis (Netzsch STA 449 F1, Germany).

2.2 Synthesis and characterization of polystyrene particles (PSs)

The polystyrene particles were prepared via emulsion polymerization by adjusting the ratios of sodium dodecylbenzenesulfonate (SDBS), styrene monomer, divinylbenzene monomer (DVB) and reaction temperature as shown in **Table 2.1**

Table 2. 1 The amount of reagents for the preparation of polystyrene particles

| Sample Names | SDBS (mg) | Styrene (mL) | DVB (mL) | Temperature (°C) |
|--------------|-----------|--------------|----------|------------------|
| PSs1 | 100 | 2.5 | 0.5 | 75 |
| PSs2 | 25.0 | 2.5 | 0.5 | 75 |
| PSs3 | 12.5 | 2.5 | 0.5 | 75 |
| PSs4 | 6.25 | 2.5 | 0.5 | 75 |
| PSs5 | 6.25 | 25 | 5.0 | 75 |
| PSs6 | 0.00 | 5.0 | 0.5 | 60 |
| PSs7 | 0.00 | 10 | 1.0 | 60 |

The SDBS (amount as shown in **Table 2.1**) was dissolved in 50 mL of deionized water under nitrogen atmosphere. The SDBS solution was stirred at the room temperature, 100 rpm for 15 min. The styrene monomer and DVB (**Table 2.1**) were added into the stirring solution at the specific temperature (**Table 2.1**) and stirring was continued for another 5 min at the same temperature. After that, 100 mg of potassium persulfate ($K_2S_2O_8$) in 50 mL of deionized water was added. After stirring 8 hr at the reaction temperature, the reaction was terminated by adding 150 ml of ethanol. After that, the sample was dialyzed using dialysis cellulose membrane (MWCO = 12-14 kDa) against deionized water. After that, the suspension in the dialysis bag was collected and dried via freeze-drying technique to obtained polystyrene particles.

2.3 Synthesis and characterization of hyper crosslink-polystyrene particles (HC-PSs)

The hyper crosslink-polystyrene particles (HC-PSs) were prepared from the obtained polystyrene particles (PSs, from 2.2). Firstly, the PSs (1.0 g) was dispersed in 30 mL of chloroform and stirred for 5 minutes. After that, the suspension was sonicated at 40 kHz at room temperature for 30 minutes until white milky suspension was obtained. The obtained suspension was heated to 75 °C. Then, aluminum trichloride (AlCl₃, 2.80g) was added into suspension. The mixture was refluxed for specific time (Table 2.2). To stop the reaction, 25 ml of 1 molar of hydrochloric (1M HCl, aq.) and 25 ml of acetone were slowly added into reaction. Then, the mixture was evaporated to remove CHCl₃, the products were then washed by 1M HCl (aq.), deionized water and acetone respectively. The obtained HC-PSs were kept in a desiccator.

Table 2. 2 The specific experiment time for hyper crosslink-polystyrene reaction.

| PS particles used as starting material | Products Names | Reaction time (hr.) |
|--|----------------|---------------------|
| PSs1 | HC-PSs1 | 24 |
| PSs2 | HC-PSs2 | 24 |
| PSs3 | HC-PSs3 | 24 |
| PSs4 | HC-PSs4 | 52 |
| PSs5 | HC-PSs5 | 52 |
| PSs6 | HC-PSs6 | 52 |
| PSs7 | HC-PSs7 | 90 |

2.4 Synthesis and characterization of carbon nanosphere particle (C)

Melamine powder (1,3,5-Triazine-2,4,6,-triamine, 15.0g) was mixed with 3.0 g of HC-PS particles (from 2.3) and placed in the chamber of the furnace. Then, the mixture was heated at 300°C for 20 minutes and the temperature was increased to 700°C for 160 minutes under nitrogen atmosphere [22]. The resulting carbon (C) was kept in a desiccator.

2.5 Synthesis and characterization of oxidized carbon particles (OPs)

The oxidized carbon particles (OPs) were prepared using modified exfoliation/oxidation process^{14-15, 17}. The conditions of oxidization were optimized by adjusting the ratio between oxidizing agent and carbon particles (from 2.3). Firstly, carbon particles were mixed with sodium nitrate (NaNO_3 , amount as shown in Table 2.4). Then, the mixture was dispersed in 18 M sulfuric acid (H_2SO_4 , amount as shown in Table 2.3). After that, the mixture was sonicated at 40 kHz at room temperature (sonication time as shown in Table 2.3). Then, potassium permanganate (KMnO_4) was slowly added into the mixture and the mixture was stirred for 90 min. Next, 50 mL of distilled water was added and stirred for another 90 min. After that, 150 mL of distilled water and 5% (w/v) of hydrogen peroxide (50 mL) was added respectively and stirred at room temperature for another 30 min. Finally, the obtained products were washed 3 times with water using centrifugation at 37,600 g (20,000 rpm). The pellet was collected, re-dispersed in water and dialyzed against deionized water with dialysis cellulose membrane (MWCO = 12-14 kDa) until pH 5.5.

Table 2. 3 The amount of reagent for the oxidation reaction of carbon particles

| Selected carbon as starting material | Conditions | | | | | Products Names |
|--------------------------------------|------------|-----------------------|------------------------|--|-----------------------|--------------------|
| | Carbon (g) | NaNO ₃ (g) | Sonication Time (min.) | 18 M H ₂ SO ₄ (mL) | KMnO ₄ (g) | |
| C1 | 0.5 | 0.5 | 60 | 25 | 3 | OP1.1 ^a |
| | 0.5 | 0 | 0 | 12.5 | 0.75 | OP1.2 |
| | 0.5 | 0 | 60 | 12.5 | 0.375 | OP1.3 |
| | 0.5 | 0.0625 | 60 | 12.5 | 0.375 | OP1.4 |
| C3 | 0.5 | 0.5 | 60 | 25 | 3 | OP3.1 ^a |
| C7 | 0.5 | 0.5 | 60 | 25 | 3 | OP7.1 ^a |

^a Referent condition ¹⁴

2.6 Effect of particles size of oxidized carbon particles on their ability to induce a leakage on lipid bilayer membrane

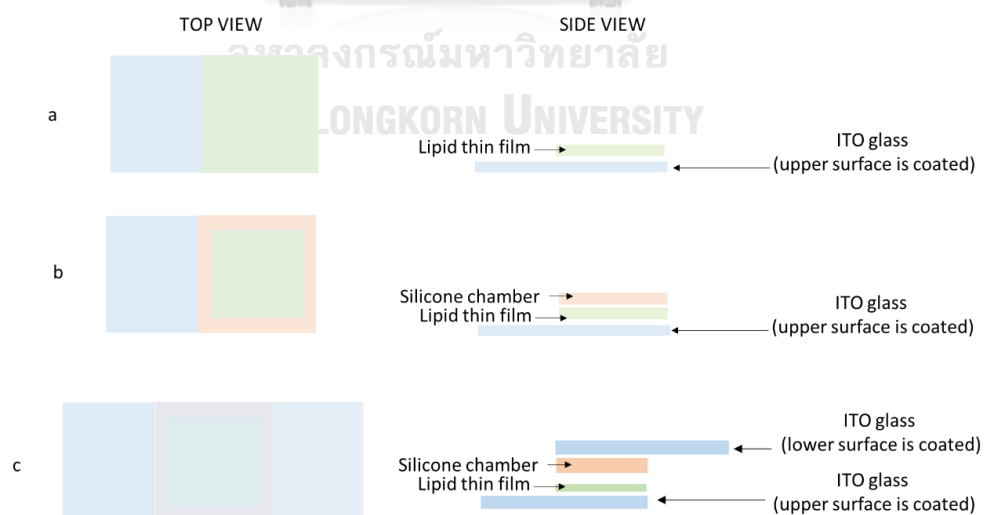


Figure 2. 1 The layer of the lipid film, chamber, and ITO-glass for liposome preparation by electroformation method

Cell-sized liposomes were prepared by electroformation method²⁴ from 1,2-dioleoyl-sn-glycero-3-phosphocholine (DOPC). Firstly, 50 μ L of 20 mM lipid solution in chloroform was coated on the conducting face of an indium tin oxide-slide glass (ITO-glass) which electrical resistance of ITO-glass was 30-40 Ω as shown in **Figure 2.1, a**. After that, the film was heated at 50°C for 5 min. Then, 30 μ L chloroform was added to spread the thin to obtain a thin film and dried in a vacuum pump for 2 hr. Next, the sample glass was cover with silicone chamber (**Figure 2.1, b**) and another conducting face of ITO-glass as shown in **Figure 2.1, c**. After that, 300 μ L of 100mM sucrose solution was injected into the chamber. Then, an alternating current of 1 volt and 10Hz (AFG-2005, Good Will Instrument Co., Ltd., Taiwan) was applied with a function generator at 50°C for 2 hr. Next, the obtained liposome suspension was carefully extracted from the chamber using a plastic syringe.

To observe the interaction between OPs and cell-sized liposome, the 20 μ L of prepared liposome suspension in water was mixed with 10 μ L of 200mM glucose solution and 30 μ L of 60 μ g/ml of oxidized carbon particles. Then, the 20 μ L of the mixture was dropped on a glass slide with a silicone chamber and observed using phase contrast microscope. To investigate the effect of incubation time on the interaction between OPs and cell-sized liposome, the phase contrast and number of liposomes were observed at 0, 30, 60, 120 and 240 min after mixing

CHAPTER III

RESULTS AND DISCUSSIONS

3.1 Synthesis and characterization of polystyrene particles (PSs)

The polystyrene particles were synthesized via emulsion polymerization. In this work, we used surfactant sodium dodecylbenzenesulfonate (SDBS) and monomer styrene and divinylbenzene (DVB). The white milky solid of sample (PSs1-PSs7) were obtained. The morphology and diameter size of PSs1-PSs7 were investigated by Scanning Electron Microscope (SEM).

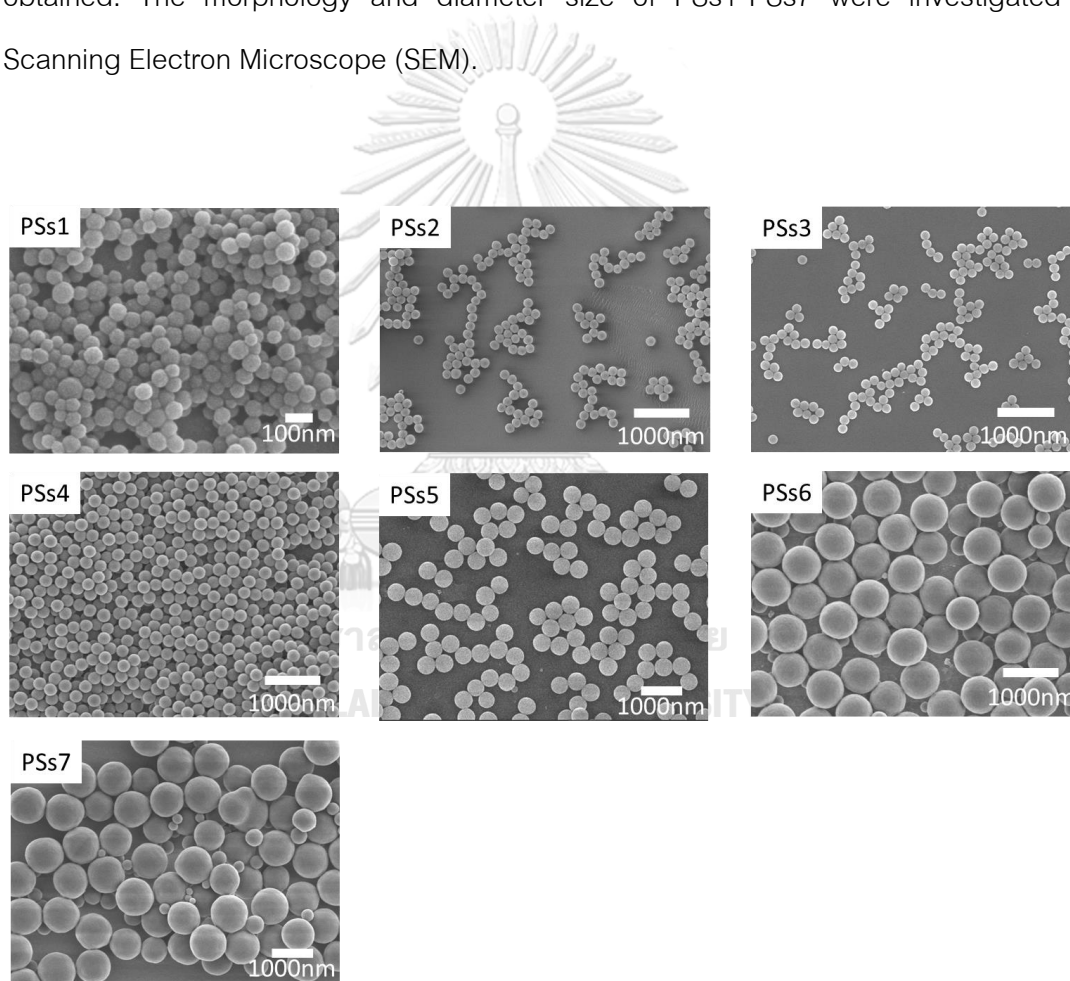


Figure 3. 1 Morphology of all PSs were prepared under different conditions

Table 3. 1 Size of PSs were prepared under different conditions

| Sample Names | SDBS (mg) | Styrene (mL) | DVB (mL) | Temperature (°C) | SEM size (nm) ^a |
|--------------|-----------|--------------|----------|------------------|----------------------------|
| PSs1 | 100 | 2.5 | 0.5 | 75 | 59±9.1 |
| PSs2 | 25 | 2.5 | 0.5 | 75 | 147±16.7 |
| PSs3 | 12.5 | 2.5 | 0.5 | 75 | 200±20.0 |
| PSs4 | 6.25 | 2.5 | 0.5 | 75 | 273±26.0 |
| PSs5 | 6.25 | 25 | 5 | 75 | 415±24.7 |
| PSs6 | 0 | 5 | 0.5 | 60 | 643±39.8 |
| PSs7 | 0 | 10 | 1 | 60 | 811±91.0 |

^a An average particles size was obtained by ImageJ analysis of SEM image

The SEM images show that all 7 PS products are spherical (Figure 3.1). The particles size of the PSs increased with decreased concentration of surfactant (PSs1-PSs4, Table 3.1) or increased concentration of monomer (comparing between PSs4 and PSs5) during the polymerization reaction. PSs6 and PSs7 were prepared in an absence of SDBS. They show a larger size of PS particles comparing with PSs1-PSs5. PSs1-PSs6 show monodisperse of polystyrene particles but PSs7 shows polydisperse.

In case of PSs1-PSs5 which were prepared in the presence of SDBS as a surfactant, the SDBS was mixed with water. After that, the monomers were added. In this step, the surfactants self-assembled into micelles by turning hydrophobic head inside the micelle and turning hydrophilic head outside to contain with water. The hydrophobic styrene and divinylbenzene mixtures stayed inside the micelles because of their hydrophobicity. After that, the added water-soluble initiator ($K_2S_2O_8$) diffused into to interfaces of micelles and water, and initiated the polymerization through the generation of free radicals as shown in Figure 3.2. In the presence of higher concentration of surfactant as used for PSs1-PSs4 preparation, a large number of smaller micelles were generated. As a result, the smaller size of particles were generated. The larger size of

PSs4 were obtained when decrease the ratio between surfactant to monomer. For explanation, when increased the concentration of monomer while the amount of surfactant was constant effected to reducing in solvate area of surfactant around monomer droplets. This system generated the larger size of micelles and after that the bigger of particles were obtained. The emulsion polymerization could give only the particles size around 50-400 nm. To prepare the bigger PS particles, PSs6 and PSs7 particles were obtained by multistage seeded polymerization in an absence of SDBS was used²³. Here, during the stirring of monomer and hot water, some monomer can get into the water and reacted with initiator. This resulted in oligomeric radical which appear as particle nucleation. When more monomer come from oil phase into water, they directly reacted these particle nucleation. This resulted in the growing from particle surface. The particles continue to grow until no more monomer come into the water phase. In this process of PSs7, we then added initiator and monomer the next day. These monomer diffuse into the water phase and react to the surface the exciting particle making them bigger. However, some monomer and initiator started the new particle nucleation. These new particles nucleation then grow into smaller particle comparing to those bigger particles. As a result, this multistate polymerization process give particle of diverse sizes²³.

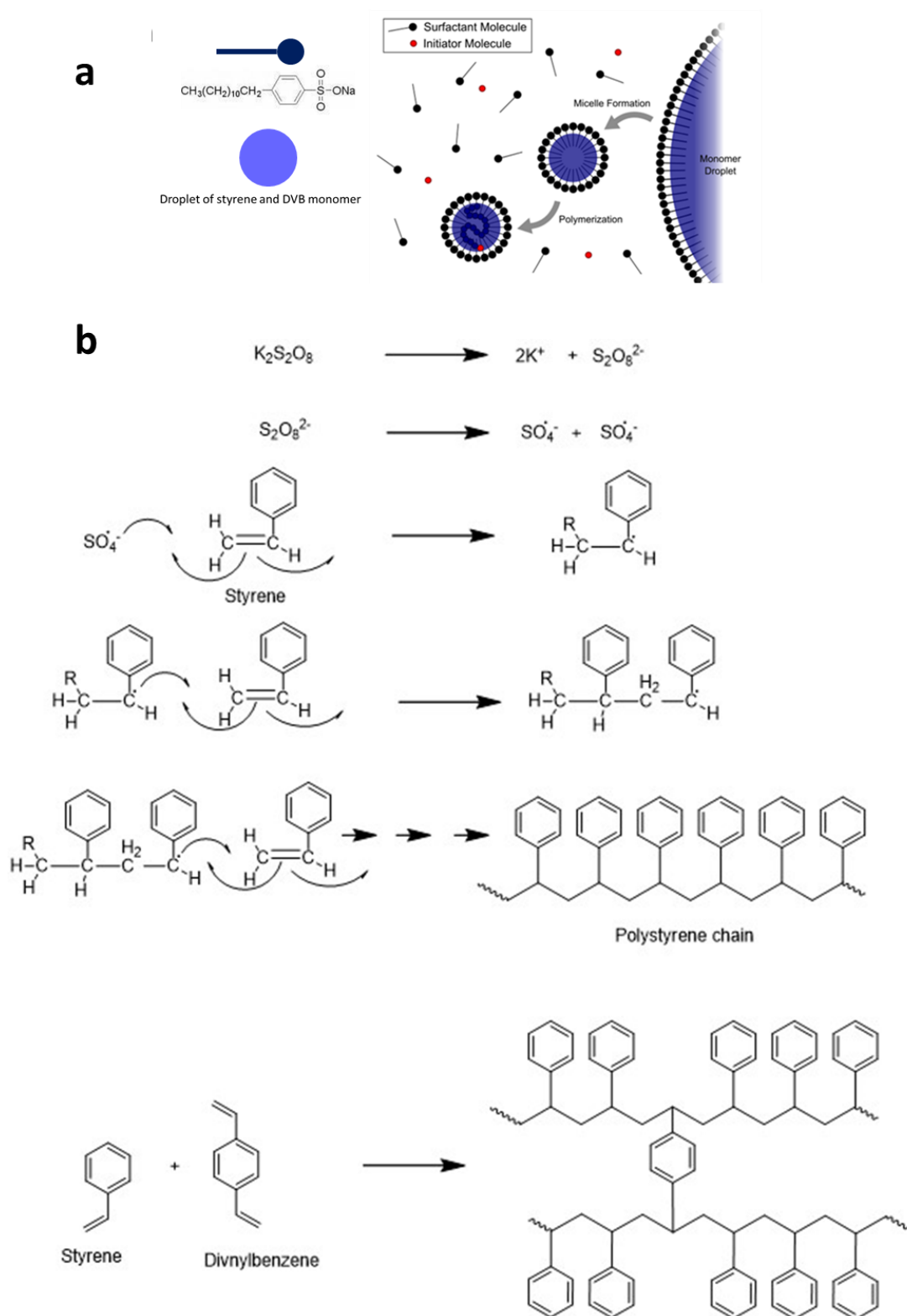


Figure 3. 2 The mechanism of emulsion polymerization (a) and polymerization mechanism of styrene and DVB monomer (b)

All PSs were characterized by Fourier-Transform Infrared Spectroscopy (FT-IR) and Thermogravimetric Analysis (TGA)

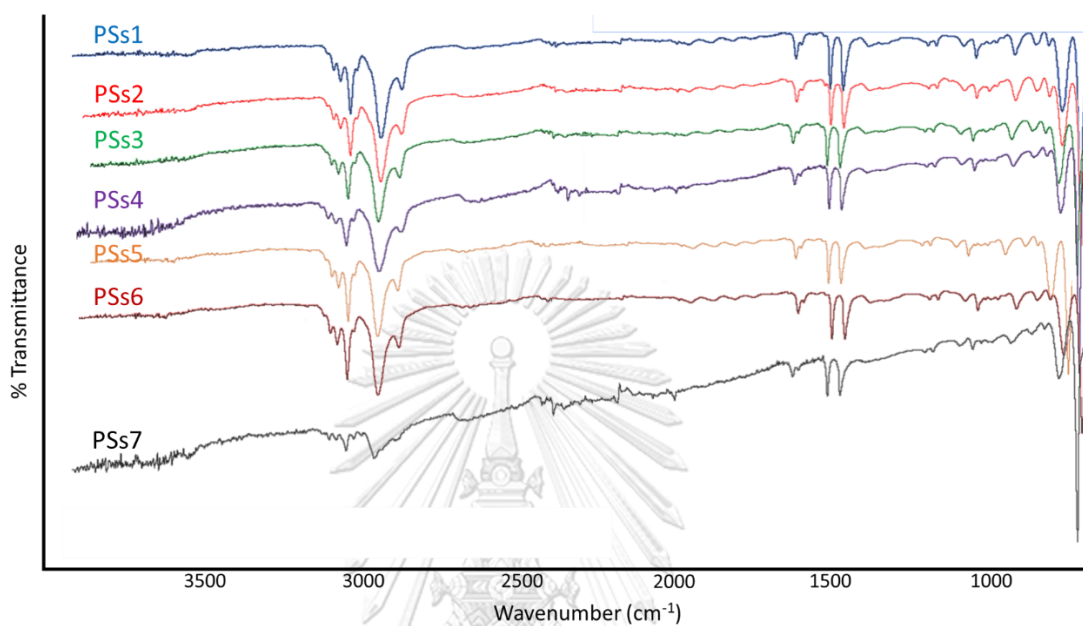


Figure 3. 3 The Fourier transform infrared (FT-IR) spectra of all PSs

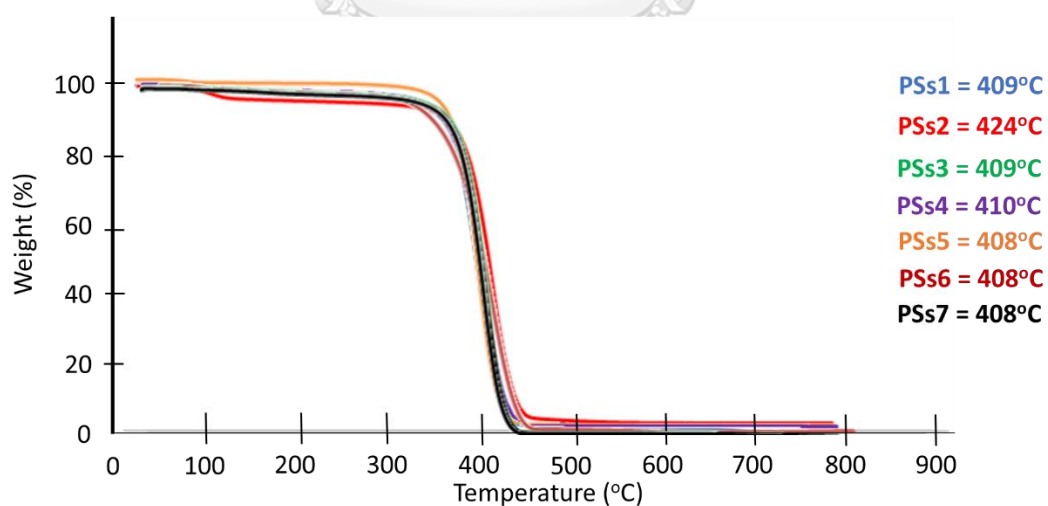


Figure 3. 4 The Thermogravimetric analysis of all PSs

FT-IR spectra of all PSs show the same pattern at 3059 and 3025 which correspond to C-H stretching of unsaturated carbon. The peak at 2912 and 1600 correspond to C-H stretching of saturated carbon and C=C stretching, respectively. The peak at 1492 and 1451 cm^{-1} correspond to C-H bending on aromatic ring. (Figure 3.3.) The thermal stability of all PSs was characterized by thermogravimetric analysis as shown in Figure 3.4. PSs1-7 show only one degradation temperature at 409°C, 424°C, 409°C, 410°C, 409°C, 407°C and 409°C, respectively and accounted for 99.79%, 92.99%, 97.12%, 98.75%, 99.47%, 99.50%, 409°C and 99.98% weight loss, respectively. All results indicated that there is one major component in the particles. The FT-IR result are a qualitative and confirmed that vibration position belongs to Polystyrene which further confirmed by reviewed literature ²⁷.

3.2 Synthesis and characterization of the hyper crosslink-polystyrene particles (HC-PSs)

After, polystyrene particles were reacted with AlCl_3 in chloroform (see method 2.3), the yellow solid particles (HC-PSs) was obtained. The morphology and diameter size of all HC-PSs were examined by SEM.

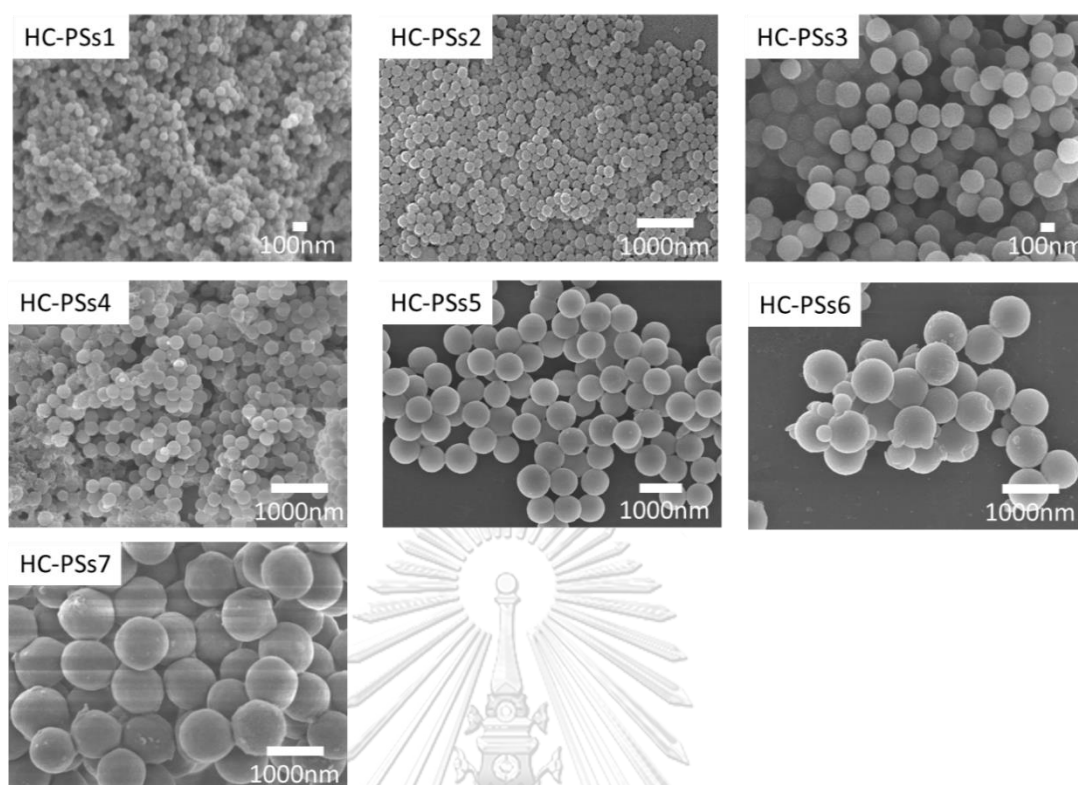


Figure 3. 5 Morphology characterization of HC-PSs prepared under different conditions

Table 3. 2 Size of HC-PSs prepared from PSs as starting material under a specific time.

| Starting material | SEM size of starting material (nm) ^a | Product Names | SEM size of the product (nm) ^a |
|-------------------|---|---------------|---|
| PSs1 | 59±9.1 | HC-PSs1 | 59±7.3 |
| PSs2 | 147±16.7 | HC-PSs2 | 158±14.3 |
| PSs3 | 200±20.0 | HC-PSs3 | 176±15.2 |
| PSs4 | 273±26.0 | HC-PSs4 | 240±16.1 |
| PSs5 | 415±24.7 | HC-PSs5 | 635±55.1 |
| PSs6 | 643±39.8 | HC-PSs6 | 639±171 |
| PSs7 | 811±91.0 | HC-PSs7 | 831±137 |

^aAn average particles size were obtained by ImageJ analysis of SEM image

The SEM images show that the morphology of HC-PSs is spherical shaped, and their sizes are similar to their corresponding PSs starting materials (Table 3.2 and Figure 3.5).

All HC-PSs were characterized by FT-IR and TGA.

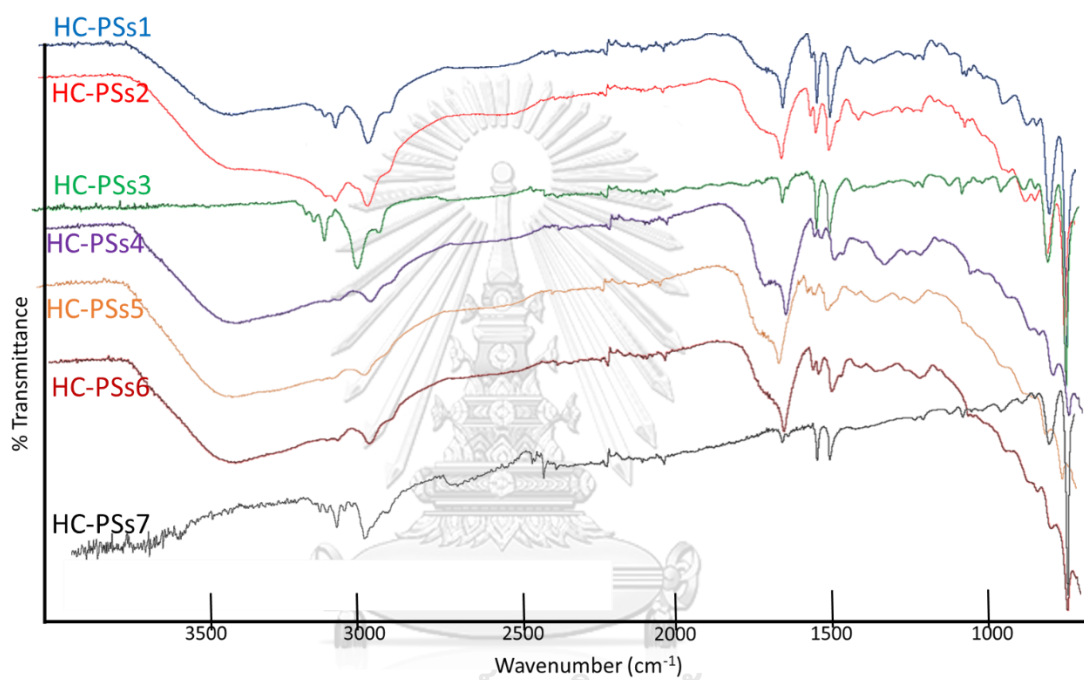


Figure 3. 6 The Fourier transform infrared (FT-IR) spectra of all HC-PSs.

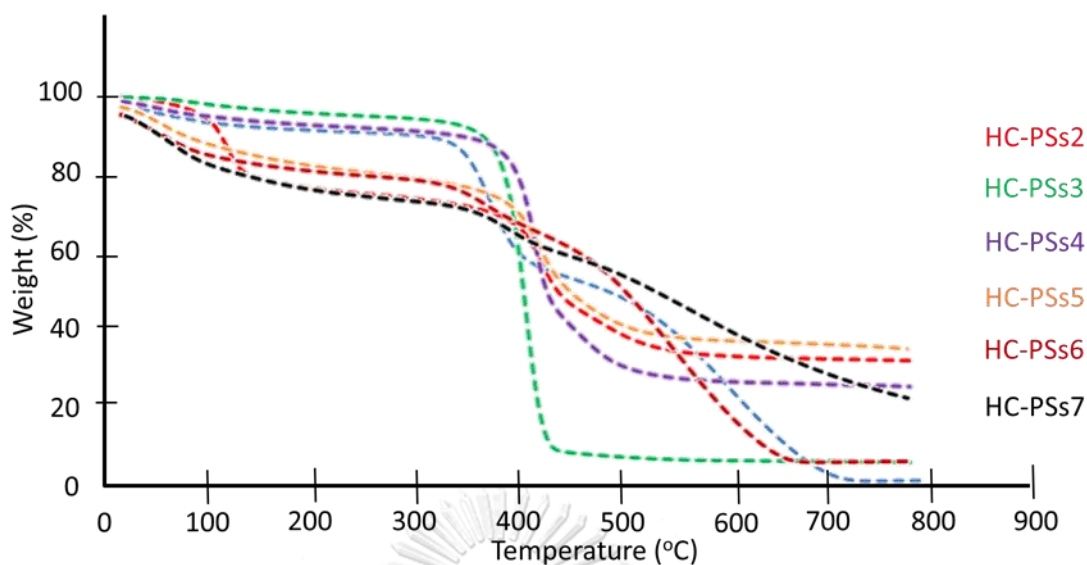


Figure 3. 7 The Thermogravimetric analysis of all HC-PSs.

FT-IR spectra of all PSs show the same pattern at 3059 and 3025 which correspond to C-H stretching of unsaturated carbon. The peak at 2912 and 1600 correspond to C-H stretching of saturated carbon and C=C stretching, respectively. The peak at 1492 and 1451 cm^{-1} correspond to C-H bending on aromatic ring as shown in Figure 3.5. The thermal stability of all HC-PSs were characterized by thermogravimetric analysis. HC-PSs1 shows degradation temperature at 374°C and 604°C accounted for 44.99% and 51.95% weight loss. HC-PSs2 shows degradation temperature at 132°C and 442°C accounted for 25.51% and 42.13% weight loss. HC-PSs 3-5 show only one degradation temperature at 423°C, 432°C, and 440°C, respectively and accounted for 92.97%, 75.52% and 46.74% weight loss, respectively HC-PSs6 shows degradation temperature at 387°C and 577°C accounted for 16.55% and 57.85% weight loss. HC-PSs7 shows degradation temperature at 406°C and 601°C accounted for 15.01% and 36.51% weight loss.

FT-IR spectra of the obtained HC-PSs are similar to those of the un-crosslinked PS particles (Figure 3.3). The degradation temperature shifts of HC-PSs to a higher

temperature as compared to their parent PSs. The peak shifting of HC-PSs indicated the chemical modification of HC-PSs. The degradation temperature at 374, 387 and 406°C which are HC-PSs1, HC-PSs6 and HC-PSs7, respectively probably are excess polystyrene particles. The result agrees to the crosslinking among polymer chains via Friedel-Craft alkylation²¹. The mechanism is proposed as following: 1) Chloroform (CHCl_3) reacts with Lewis acid (AlCl_3) to form a carbocation on the benzene ring, 2) the loss of the halide leaving group to give the electrophilic alkyl carbocation and the pi electrons of the aromatic $\text{C}=\text{C}$ act as a nucleophile and attack the electrophilic carbocation, 4) the aromaticity is destroyed in this step giving the cyclohexadienyl cation intermediate, 5) rearomatization of cyclohexadienyl cation to obtain an aromatic system (Figure 3.8).

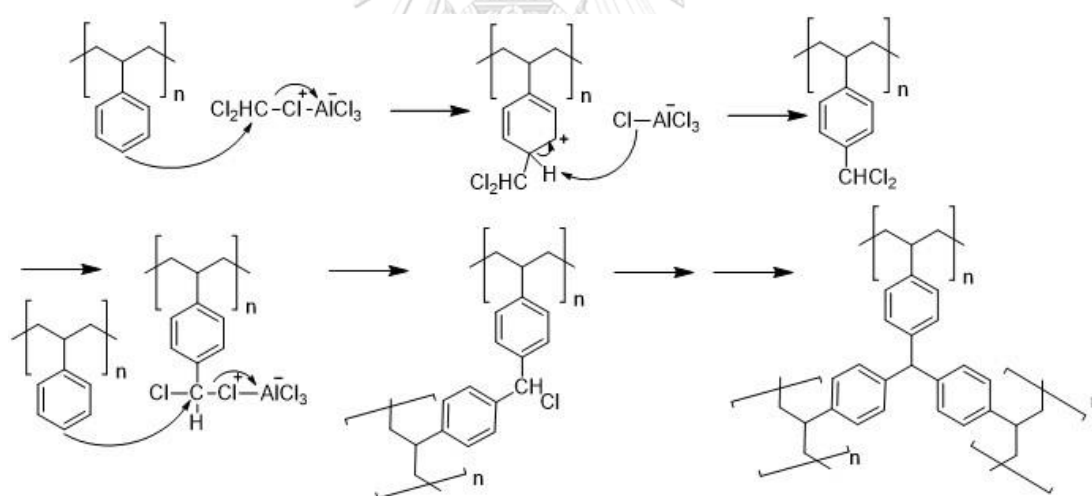


Figure 3. 8 The mechanism of hyper crosslink-polystyrene particles via Friedel-Craft alkylation

3.3 Synthesis and characterization of carbon nanosphere particles (C)

From pyrolysis HC-PSs in the presence of melamine (see 2.1). Power black solid product there are name C1-C7 were obtained. The morphology of all the products were examined by SEM.

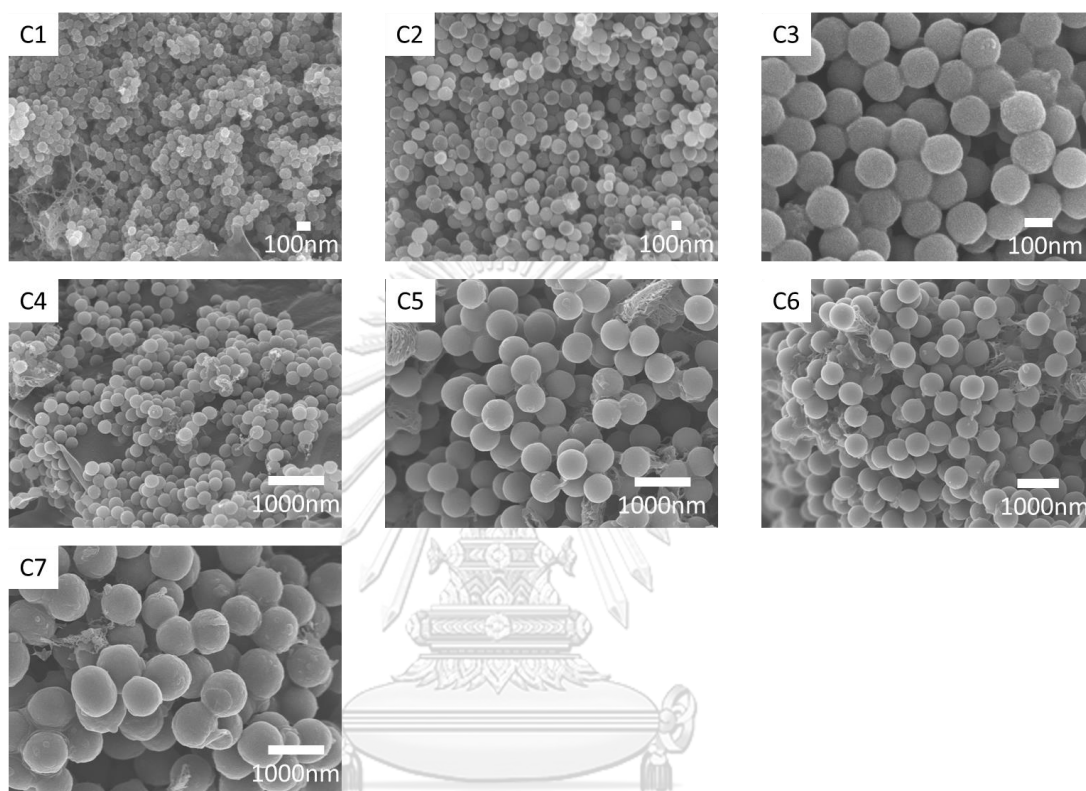


Figure 3. 9 Morphology characterization of all products prepared from pyrolytic carbonization

Table 3. 3 Size of all products prepared by pyrolytic carbonization under different time conditions.

| Starting material | Products | SEM size (nm) ^a |
|-------------------|----------|----------------------------|
| HC-PSs1 | C1 | 56±10 |
| HC-PSs2 | C2 | 140±17.8 |
| HC-PSs3 | C3 | 156±12.4 |
| HC-PSs4 | C4 | 246±16.2 |
| HC-PSs5 | C5 | 538±32.0 |
| HC-PSs6 | C6 | 556±44.3 |
| HC-PSs7 | C7 | 820±49.7 |

^a An average particles size were obtained by ImageJ analysis of SEM image

The SEM images of C1-C7 which was pyrolyzed at 700°C in the presence of melamine show spherical shape of particles and the sizes of the obtained particles are not significantly different from the HC-PSs and PSs particles. (Table 3.3 and Figure 3.9)

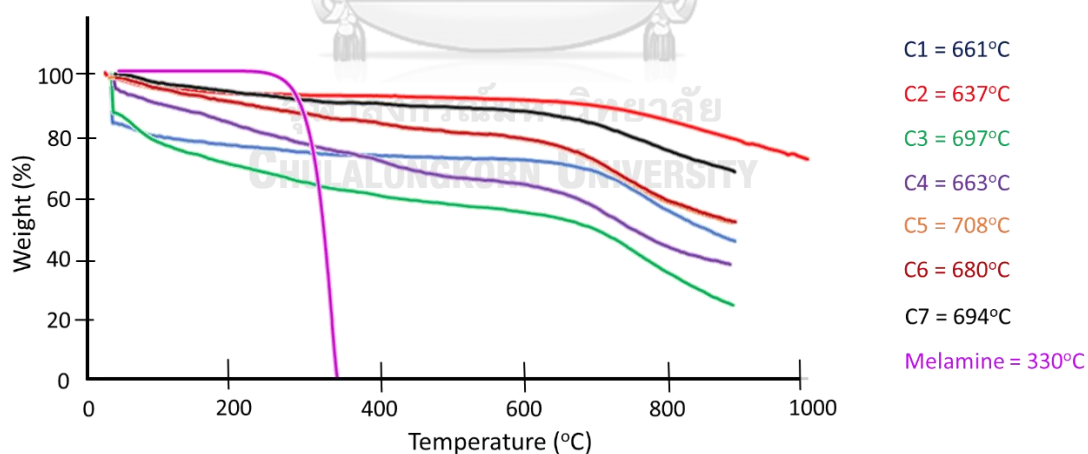


Figure 3. 10 The Thermogravimetric analysis of all products prepared from pyrolytic carbonization

TGA of C1-C7 are shown in Figure 3.10, the C1-C7 degraded at 637.7-708.0 °C. The degradation temperature of the products which are significantly higher than the degradation temperature of their corresponding HC-PSs. The degradation temperature of melamine monomers (392.5°C) is not observed in thermogram of carbon samples.

The TGA results indicated the products prepared from pyrolytic carbonization has no excess melamine monomers after pyrolytic process. The thermal degradation shifting of products confirm the chemical modification of carbon.

Here, the chemical functional group of all carbon samples were analyzed by the following techniques.

- 1.) The Fourier transform infrared (FT-IR) spectroscopy

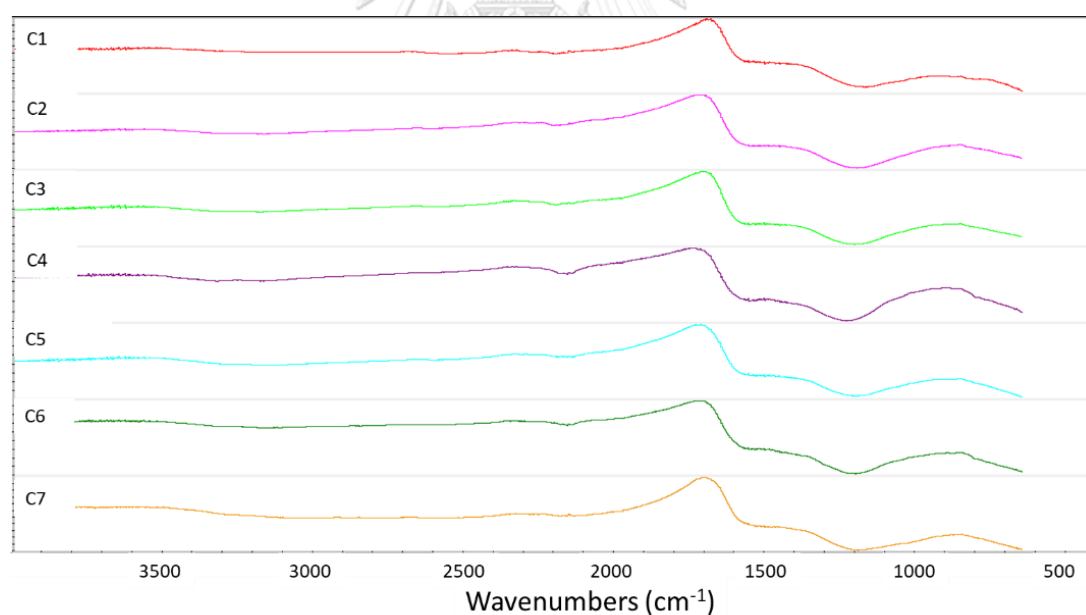


Figure 3. 11 The FT-IR spectra of all products prepared from pyrolytic carbonization

From their FT-IR result, C1-C7 have no peaks at 3059, 3025, 2912, 1600, 1492 and 1451 cm^{-1} which correspond to C-H stretching of saturated carbon, C-H stretching of unsaturated carbon, C=C stretching and C-H bending, respectively in their spectrum.

These indicated that possible successful pyrolysis. The resulting particle no amount of hydrogen atom. Their FT-IR also show peaks at 2359, 1550, and 1200 cm^{-1} which correspond to $\text{C}\equiv\text{N}$, $\text{C}=\text{C}$ and $\text{C}-\text{N}$, respectively (Figure 3.11).

2.) Raman spectroscopy

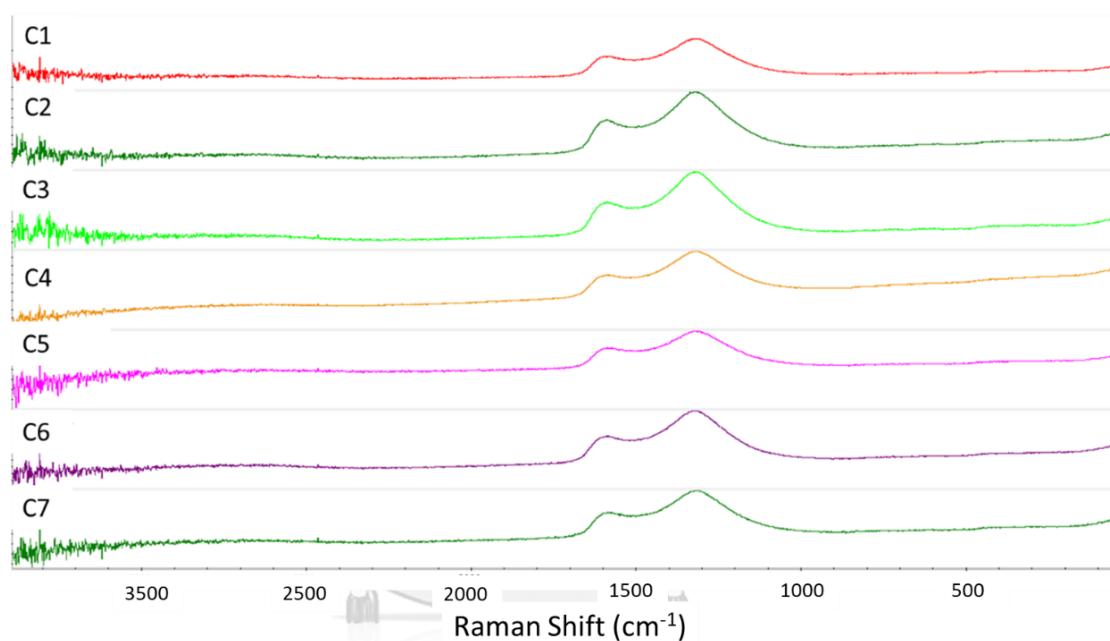


Figure 3. 12 The Raman spectrums of all products prepared from pyrolytic carbonization

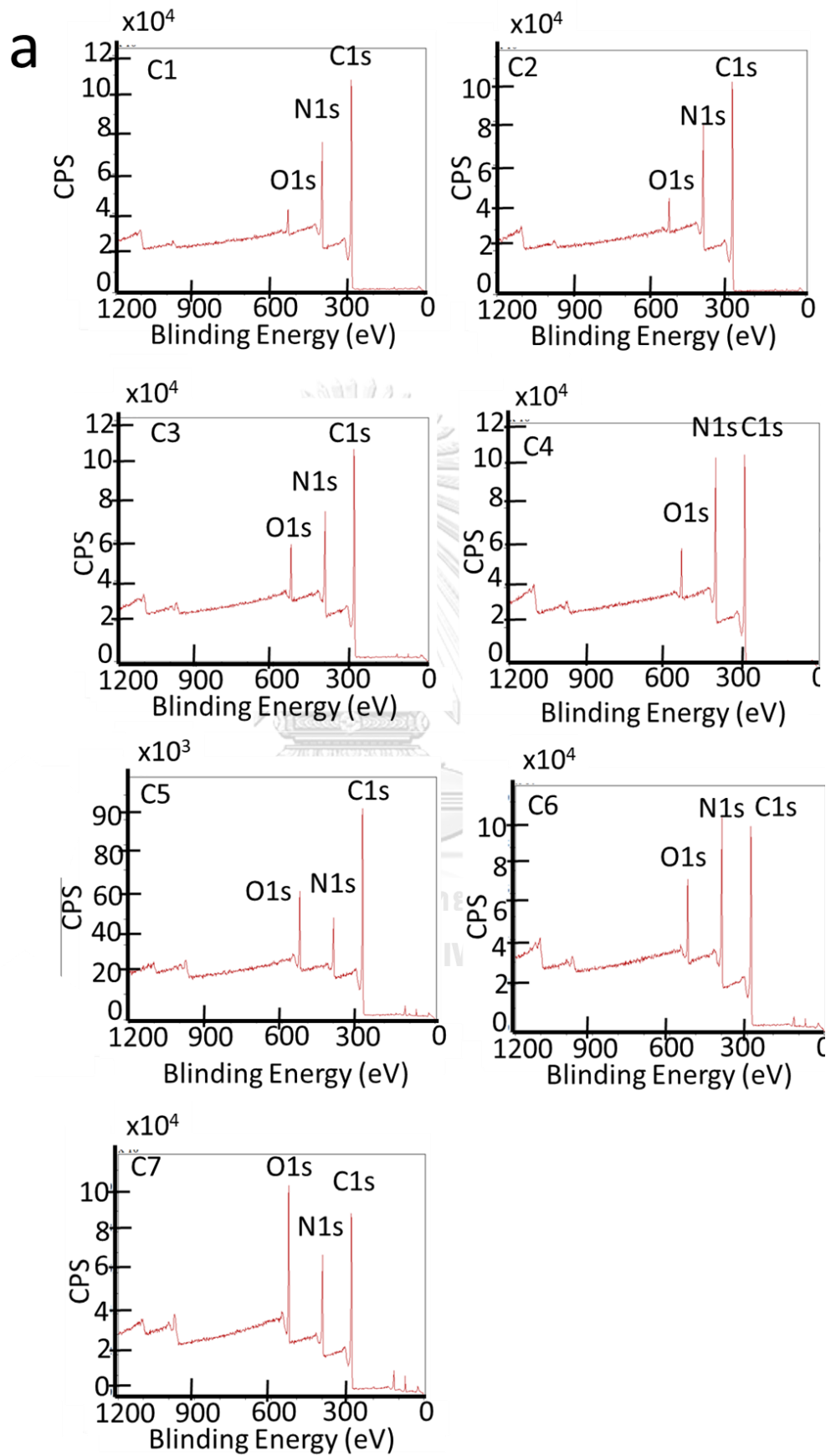
The Raman spectrum also agree well with their carbon network as their main structure, i.e., their spectrum show peaks at 1,360 and 1,590 cm^{-1} corresponding to D-band which indicate structural defects and partially disordered structure of sp^2 carbon, and G-band which associated with the first-order scattering of sp^2 carbon (graphite peak), respectively. The intensity of the D-band peak is higher than that of the G-band, indicating the majority of sp^2 carbons are disorder state. We speculated that nitrogen

atom (from melamine monomer) probably incorporate themselves into the sp^2 carbon network.

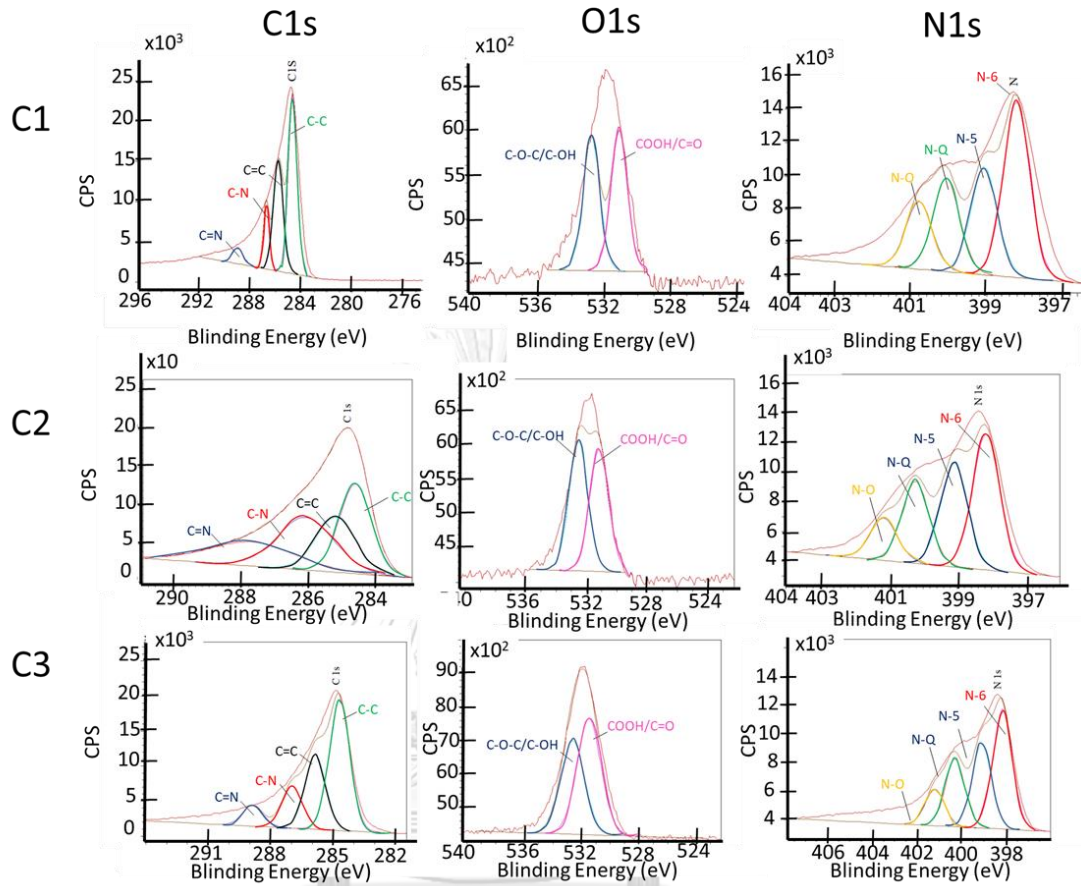
3.) X-ray photoelectron spectroscopy (XPS)

The XPS is a surface-sensitive quantitative spectroscopic technique that measures the elemental composition using binding energy value. Each functional group produced a characteristic set of XPS peaks at characteristic binding energy value. To characterized functional group on the surface of all carbon samples, XPS was used.





b



C

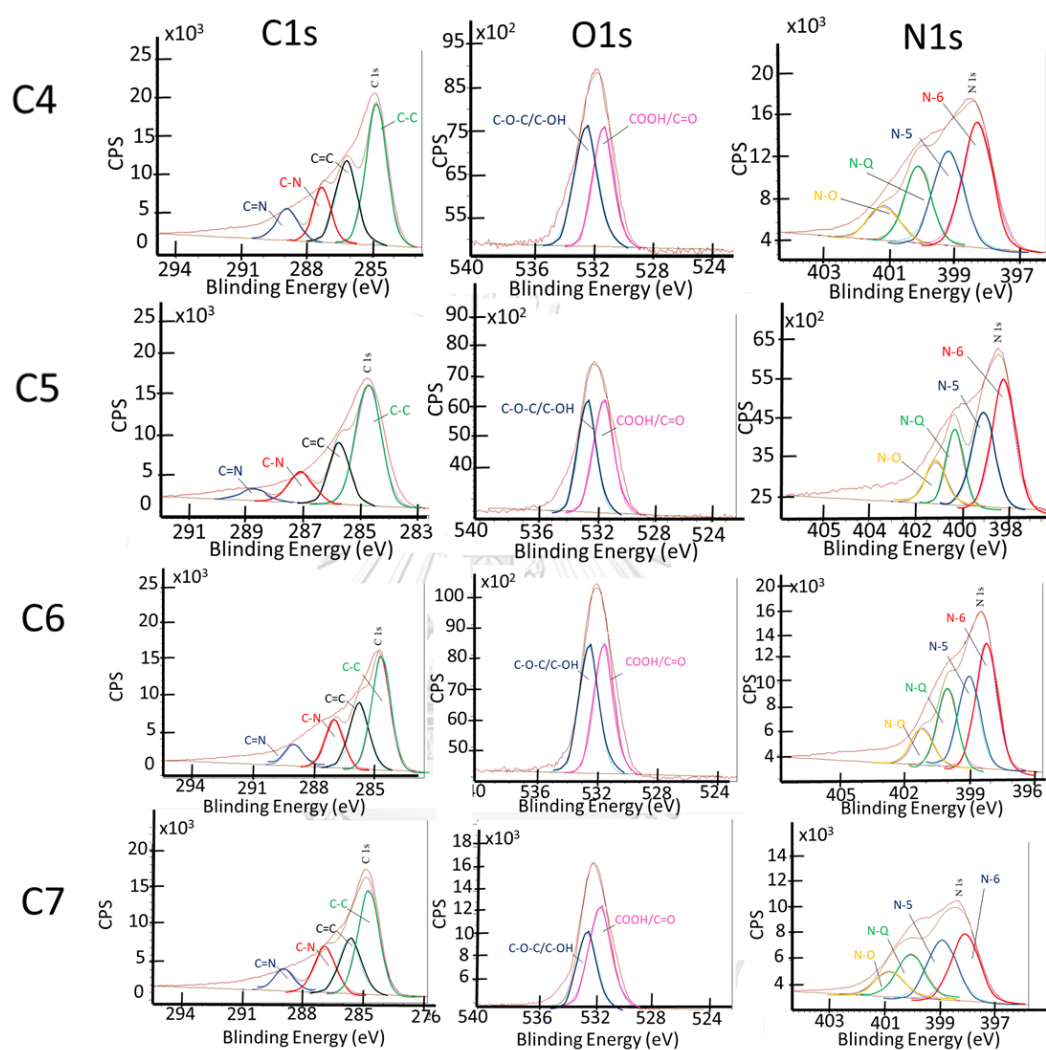


Figure 3.13 The XPS spectrum of all carbon samples, survey scan spectra (a) and deconvolutes C1s, O1s and N1s fitting spectra (b and c)

The survey scan XPS spectra of carbon samples show C1s, O1s, and N1s absorption peaks (Figure 3.13, a). Deconvolution of C1s peak (Figure 3.13, b and c) reveal components which corresponded to the binding energy of 284.7, 285.5, 286.7 and 288.99 eV which can be related to C-C, C=C, C-N, and C=N bonding, respectively.

Deconvolution of O1s peak reveal components which corresponded to the binding energy of 530.9 and 532.8 eV. which can be related to the C=O in the COOH and C-O-C/C-OH bonding, respectively. The deconvolution of N1s peak (Figure 3.13, b and c) reveal components which corresponded to the binding energy of at 398.3, 399.0, 400.0 and 400.79 eV which can be related to pyridinic nitrogen, where the N has sp^2 hybridization with two C atom (N-6), the pyrrolic nitrogen where N in five-membered ring of C atom (N-5), the quaternary nitrogen which substitutes carbon atom in graphene layer (N-Q) and the pyridine oxide, respectively ²¹.

The presence of C-N, C=N, N-6, N-5 and N-Q in the carbon particle structure implied from their XPS spectra, agreed well with our previous speculation on the incorporation of N atom into the sp^2 carbon network. It is likely that when being heated carbon nitride species were generated from melamine monomer. The nitride species were further decomposed into nitrogen atoms which then diffused into carbon networks

²¹

3.4 Synthesis and characterization of oxidized carbon particles (OPs)

The C1, C3, and C7 were selected as starting materials for further oxidation process using the mixture of KMnO_4 , H_2SO_4 , and NaNO_3 .

3.4.1 Oxidized carbon particles from C1

The amounts of oxidizing agents are optimized in oxidation reaction of C1 as shown in Table 3.4

Table 3. 4 The amount of reagent for the oxidation reaction of C1 (carbon particles)

| Selected carbon as starting material | Conditions | | | | | Products Names |
|--------------------------------------|------------|---------------------|------------------------|-----------------------------------|---------------------|--------------------|
| | Carbon (g) | NaNO_3 (g) | Sonication Time (min.) | 18 M H_2SO_4 (mL) | KMnO_4 (g) | |
| C1 | 0.5 | 0.5 | 60 | 25 | 3 | OP1.1 ^a |
| | 0.5 | 0 | 0 | 12.5 | 0.75 | OP1.2 |
| | 0.5 | 0 | 60 | 12.5 | 0.375 | OP1.3 |
| | 0.5 | 0.0625 | 60 | 12.5 | 0.375 | OP1.4 |

^a Reference condition ¹⁴

After the C1 oxidation process, the brown suspension of oxidized carbon particles (OP1) was obtained. The morphology of all oxidized carbon particles from C1 was observed by SEM.

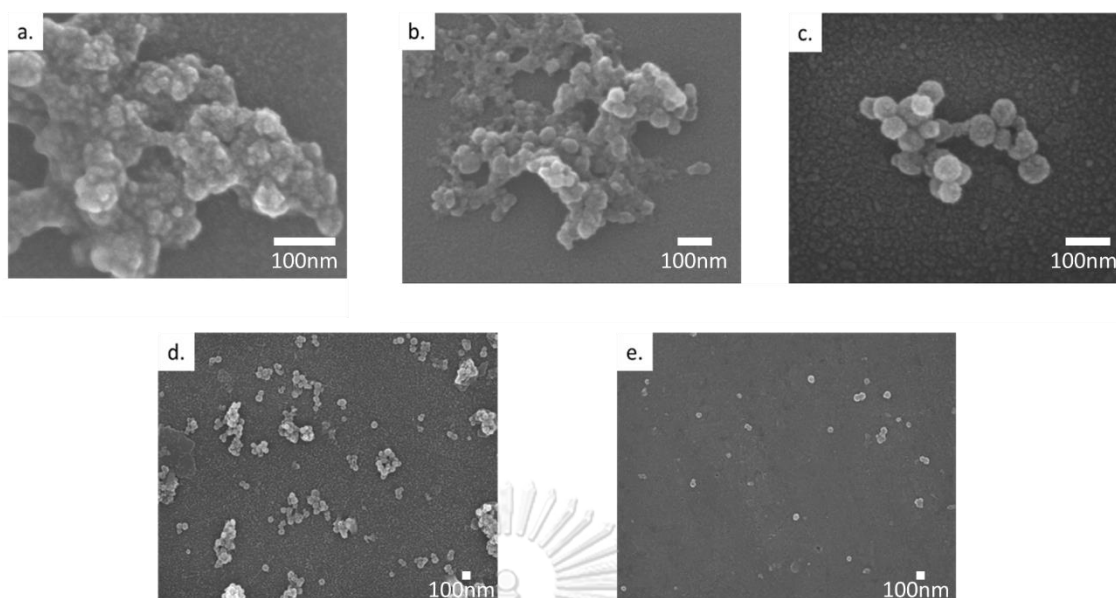


Figure 3. 14 The SEM images of oxidized carbon particles which are prepared from C1 in different conditions

The SEM image of OP1.1 shows tight aggregation of spherical particles (**Figure 3.14, a**). These particles probably come from the over oxidation of the spherical C1 particles. The SEM image of OP1.2, prepared with no NaNO_3 and sonication step (**Figure 3.14, b**) shows similar result with OP1.1, e.g., tight aggregation of spherical particles. With the reduced amount of KMnO_4 and still no NaNO_3 , the OP1.3 morphology shows less aggregation of ~ 50 nm oxidized carbon particle comparing with OP1.1 and OP1.2 (**Figure 3.14, c**). By modified preparation OP1.3 through the addition NaNO_3 , the OP1.4 morphology shows less aggregation of ~ 50 nm oxidized carbon particle comparing with OP1.1, OP1.2 and OP1.3 (**Figure 3.14, d**). In order to get completely non-aggregated oxidized carbon particles with the size 50 nm, we centrifuged suspension of OP1.4 at 37,600 g (20,000 rpm) for 30 min. The pellet was discarded, and the supernatant was collected and named OP1.5. The SEM image of OP1.5 (**Figure 3.14, e**) indeed show non-aggregated 50 nm spherical particle (**Table 3.6**). OP1.5 are well dispersed in water comparing with parent carbon particles (**Figure 3.16**). These

indicated successful functionalization by oxidation process. These OP1.5 particles were later used in membrane penetration experiment.

From the above results, it is noticeable that sonication process and NaNO_3 important to separate the particles. It probably destroyed the interactions between each carbon particles, that the OP1.4 condition was used to prepare the oxidized carbon particles from C1.

3.4.2 Oxidized carbon particles from C3

The amount of oxidizing agent for the oxidation reaction of C3 is shown in Table

3.5

Table 3. 5 The amount of reagent for the oxidation reaction of C3 and C7 (carbon particles)

| Selected carbon as starting material | Conditions | | | | | Products Names |
|--------------------------------------|------------|---------------------|------------------------|-----------------------------------|---------------------|--------------------|
| | Carbon (g) | NaNO_3 (g) | Sonication Time (min.) | 18 M H_2SO_4 (mL) | KMnO_4 (g) | |
| C3 | 0.5 | 0.5 | 60 | 25 | 3 | OP3.1 ^a |
| C7 | 0.5 | 0.5 | 60 | 25 | 3 | OP7.1 ^a |

^a Reference condition ¹⁴

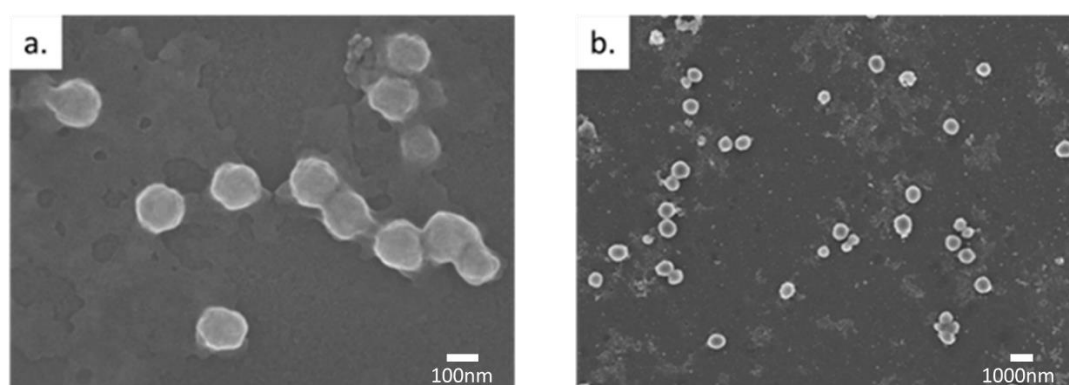


Figure 3. 15 The SEM image of the OP3.1 (a) and OP7.1 (b)

The SEM image of the OP3.1 (Figure 3.15, a) shows non-aggregated spherical particles diameter around 140 nm (Table 3.6). OP3.1 are well dispersed in water comparing with parent carbon particles (Figure 3.16). The OP3.1 was selected for further study.

3.4.3 Oxidized carbon particles from C7

The amount of oxidizing agent used during the oxidation reaction of C7 is shown in Table 3.6.

The SEM image of the OP7.1 (Figure 3.15, b) shows spherical shape and non-agglomerated particles with diameter around 700 nm (Table 3.6). OP7.1 are well dispersed in water comparing with parent carbon particles (Figure 3.16). The OP7.1 was selected for further study.

Table 3. 6 The sizes and zeta potentials of the three selected oxidized carbon particles

| Selected carbon as starting material | | Products | | |
|--------------------------------------|----------------------------|----------|----------------------------|---------------------|
| Names | SEM size (nm) ^a | Names | SEM size (nm) ^a | Zeta potential (mV) |
| C1 | 56±10 | OP1.5 | 57 ± 11 | -15.2 ± 1.41 |
| C3 | 156±12.4 | OP3.1 | 137 ± 9.49 | -30.8 ± 7.07 |
| C7 | 820±49.7 | OP7.1 | 716 ± 113 | -17.5 ± 2.13 |

^a An average particles size were obtained by ImageJ analysis of SEM image

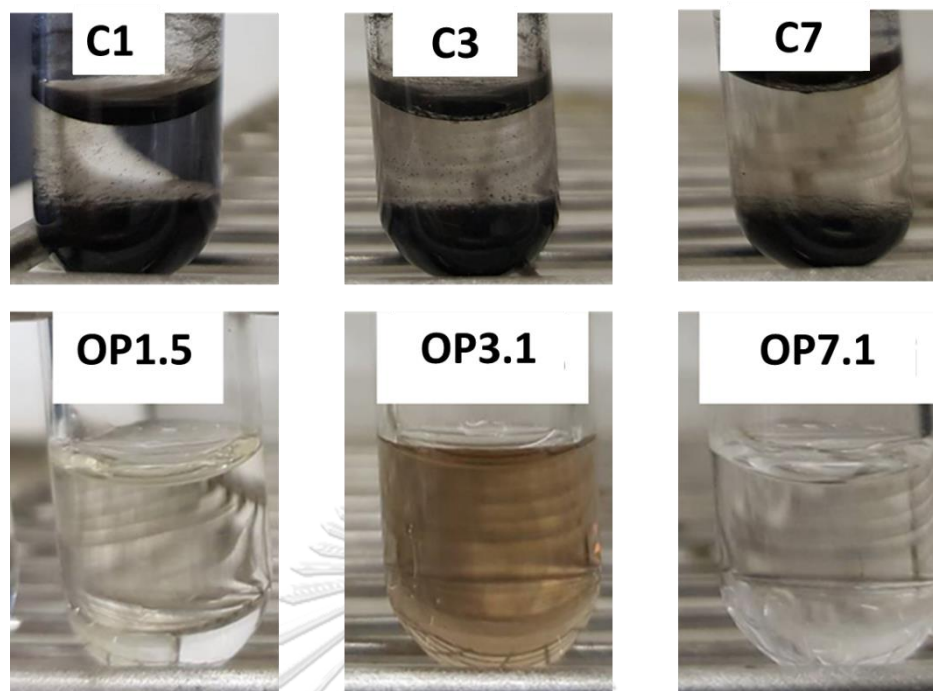


Figure 3. 16 Water dispersibility of carbon particles (top) and oxidized carbon particles (bottom)

The results show that the size of oxidized carbon particles is not significantly changed from their parent carbon particles. The optimized oxidation condition (OP1.5, OP3.1 and OP7.1) was just right that their surfaces were oxidized whereas their spherical morphology and size were preserved. The zeta potentials of oxidized carbon particles results show the negatively charged surface.

Here, the chemical functional group of selected oxidized carbon particles was analyzed by following techniques.

1.) The Fourier transform infrared (FT-IR) spectroscopy

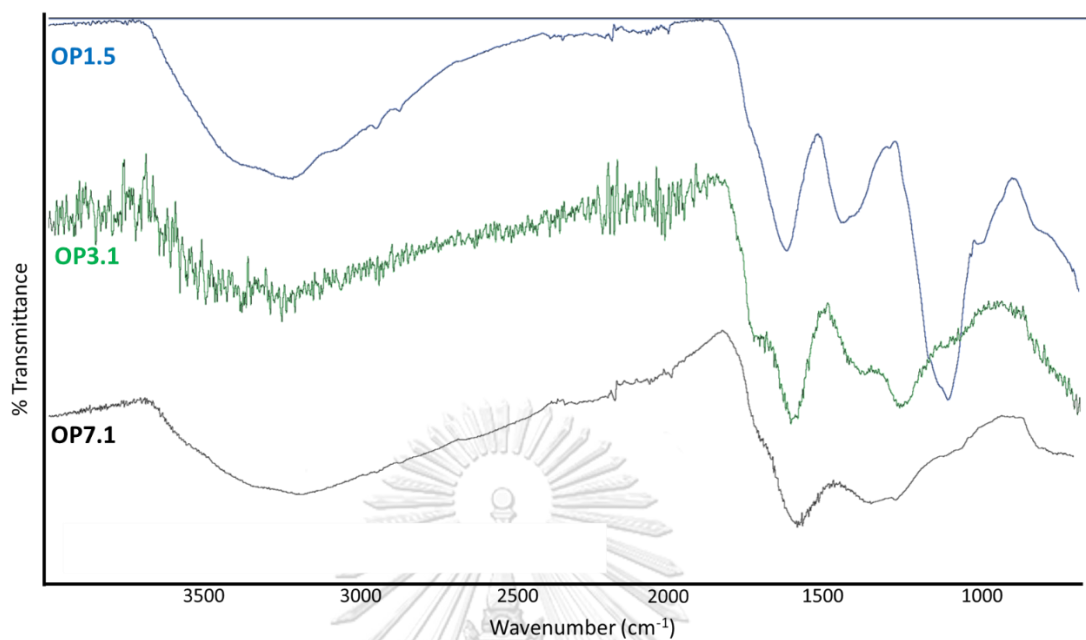


Figure 3. 17 The FT-IR spectra of all oxidized carbon particles

FT-IR spectra of OP1.5 (Figure 3.17, blue line) shows peak at 3210, 1596, 1412 and 1069 cm^{-1} which correspond to -OH stretching, C=C stretching, -OH bending of alcohol and C-O stretching of alcohol, respectively. FT-IR spectra of OP3.1 (Figure 3.17, green line) shows peak at 3300, 1732, 1599 and 1248 cm^{-1} which correspond to -OH stretching, C=O stretching, C=C stretching and C-N stretching, respectively. The FT-IR spectra of OP7.1 (Figure 3.17, black line) shows peak at 3285, 1732, 1614 and 1324 cm^{-1} which correspond to -OH stretching, C=O stretching, C=C stretching and C-O stretching of alcohol, respectively.

2.) Raman spectroscopy

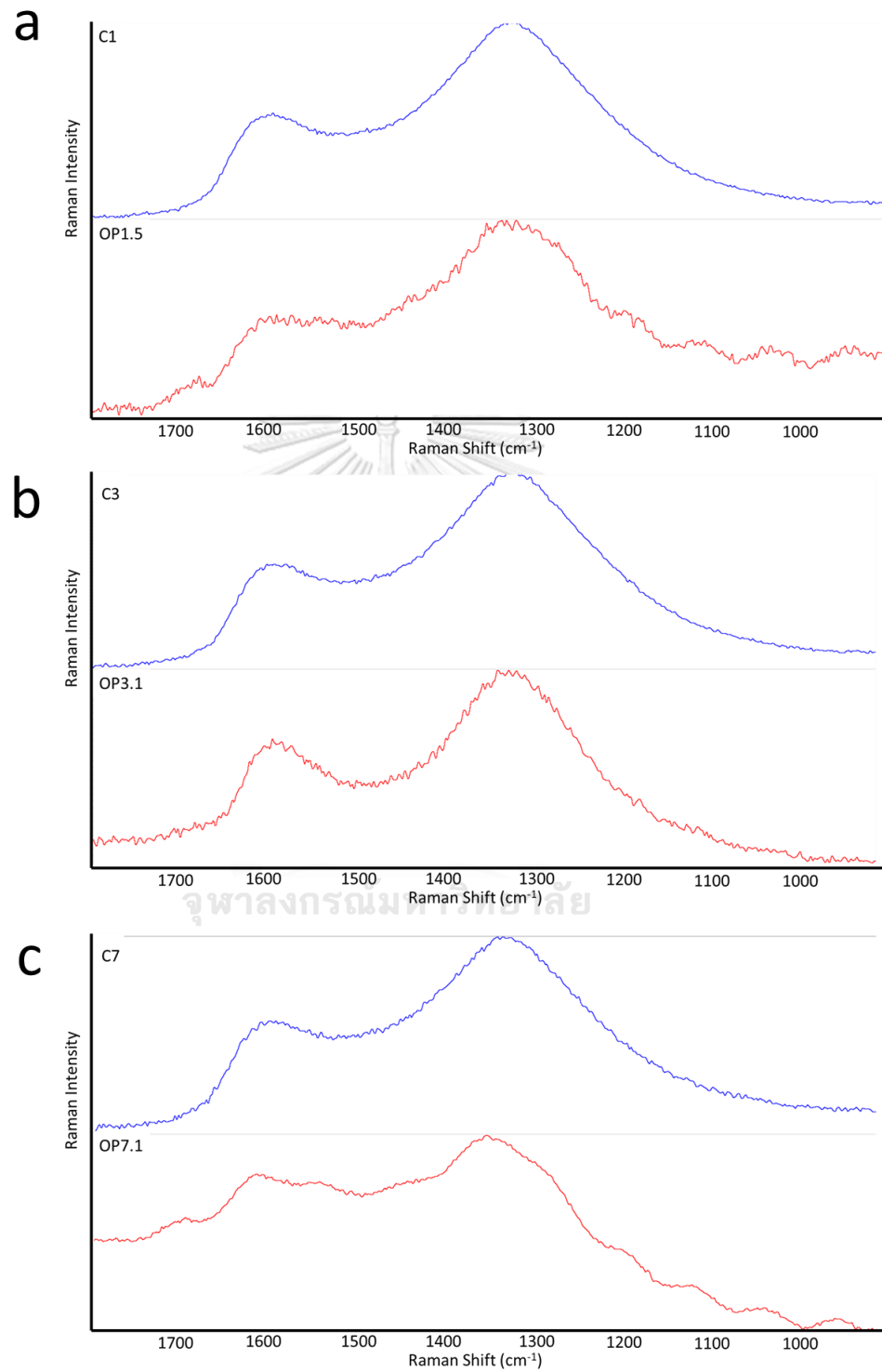


Figure 3. 18 The Raman spectra of oxidized carbon particles (red) comparing with their parent carbon particles (blue)

The Raman spectrum also agree well with their carbon network as their main structure, i.e., their spectrum show peaks at 1,360 and 1,590 cm^{-1} corresponding to D-band which indicate structural defects and partially disordered structure of sp^2 carbon, and G-band which associated with the first-order scattering of sp^2 carbon (graphite peak), respectively. In addition, the D band to G band peak area ratio decrease from 4.80 for the parent C1 to 2.15 for the OP1.5, from 4.86 for the parent C3 to 4.41 for the OP3.1 and from 4.71 for the parent C7 to 2.03 for the OP7.1.

The changes indicate the structural deformation of the planar carbon (sp^2 carbon) upon oxidation of carbon particles (C) into oxidized carbon particles (OP).

3.) X-ray photoelectron spectroscopy (XPS)

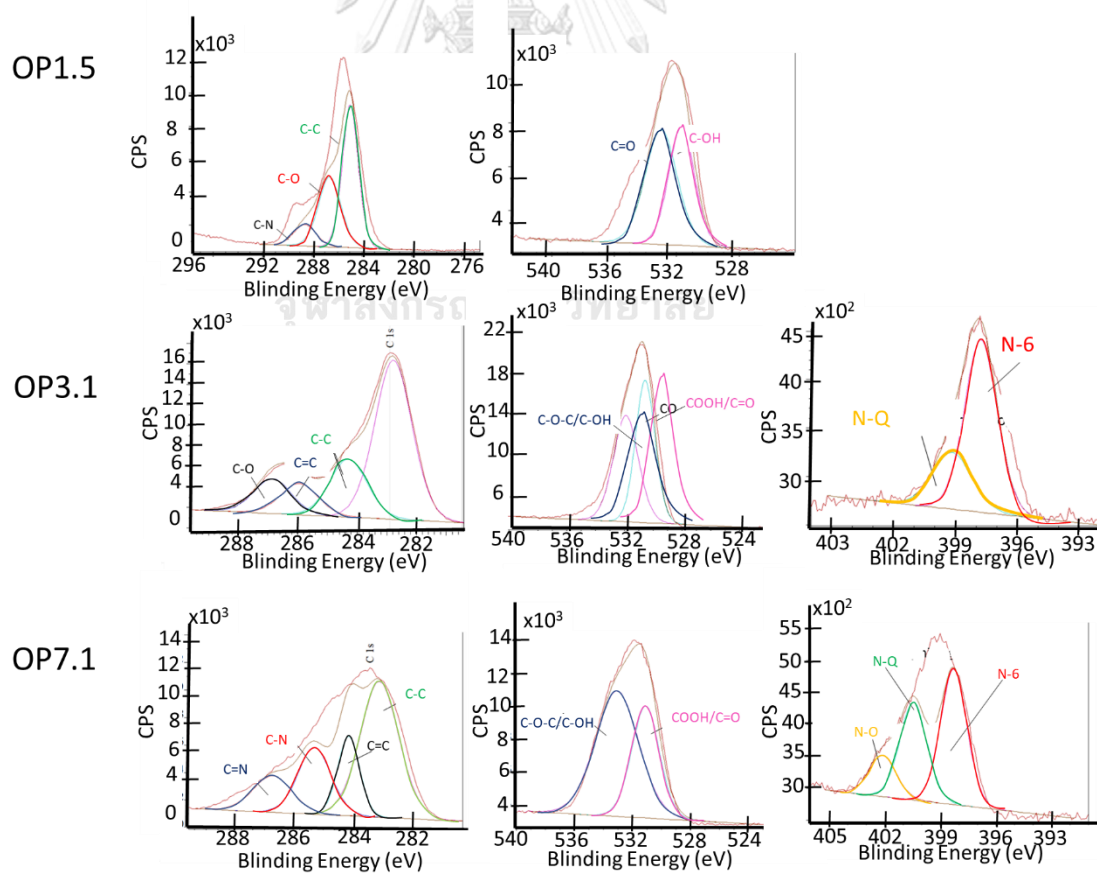


Figure 3. 19 C1s, O1s, and N1s of XPS spectra of OP1.5, OP3.1, and OP7.1

Deconvolution of C1s peak of OP1.5 reveal components which corresponded to the binding energy of 284.9, 286.7 and 288.6 eV which can be related to C=C, C-O, and C-N bonding, respectively. Deconvolution of C1s peak of OP3.1 reveal component which corresponded to the binding energy of 283.9, 285.5 and 286.7 eV which can be related to C-C, C=O, and C-O bonding, respectively. And Deconvolution of C1s peak of OP7.1 reveal component which corresponded to the binding energy of 284.5, 285.8, 287.5 and 288.8 eV which can be related to C-C, C=C, C=N, and C-N bonding, respectively. Deconvolution of O1s peak of OP1.5 reveal components which corresponded to the binding energy of 532.1 and 533.9 eV. which can be related to the C-O and C=O bonding, respectively. Deconvolution of O1s peak of OP3.1 and OP7.1 reveal component which corresponded to the binding energy of 529.1 and 531.1 eV. which can be related to the C=O in COOH and C-OH bonding, respectively. Deconvolution of N1s peak of OP3.1 reveal component which corresponded to the binding energy of at 393.3 and 399 eV which can be related to pyridinic nitrogen and quaternary nitrogen, respectively. The deconvolution of N1s peak of OP7.1 reveal components which corresponded to the binding energy of at 398.2, 399 and 402 eV which can be related to pyridinic nitrogen, quaternary nitrogen and oxidized nitrogen, respectively (Figure 3.19).

From these above results, we propose that under an appreciate oxidation condition, aggregated spherical carbon particles of C1, C3 and C7 could be dimociated and surface oxidized simultaneously. Various hydrophilic functional groups such as C=O, -COOH, -OH arise from surface oxidation and enable the particles to disperse well in water.

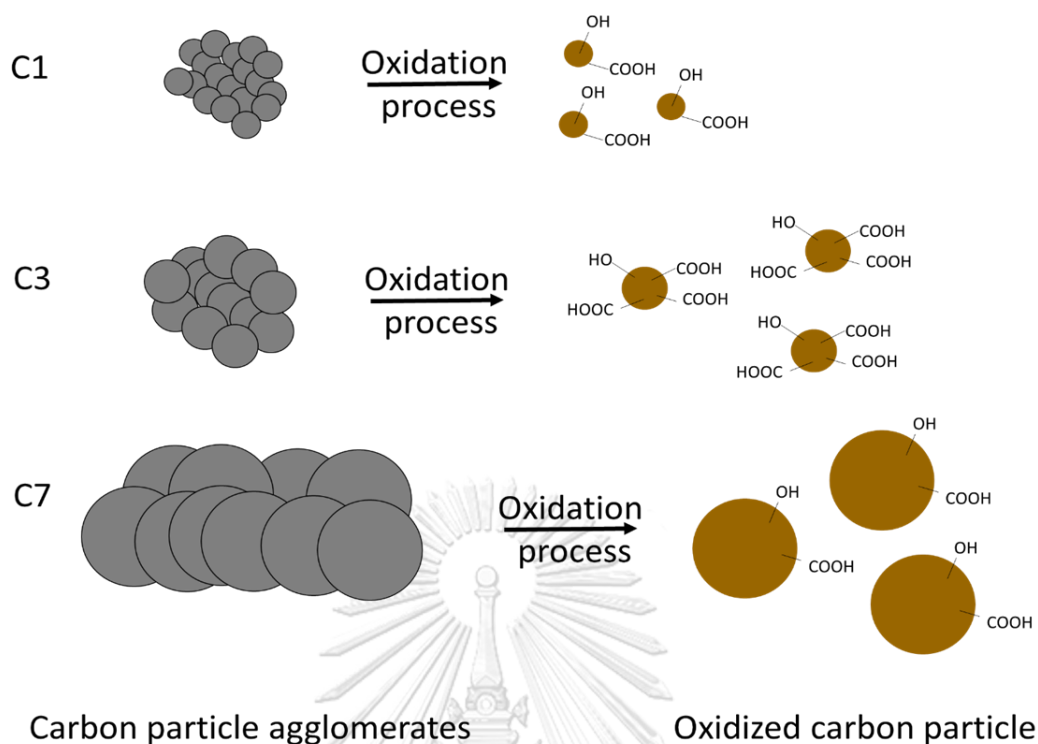


Figure 3. 20 A shortened scheme of the proposed mechanism of oxidation of carbon particles

3.5 Effect of particles size of oxidized carbon particles on their ability to induce a leakage on lipid bilayer membrane

The effect of particles size of oxidized carbon particles on the ability to induce lipid membrane leakage was investigated by incubating oxidized carbon particles with the artificial cell (cell-sized liposome) constructed from phospholipids that commonly found in the membrane of living cells²⁸. The experiment was started by adding glucose solution with liposome suspension under an observation by phase contrast microscope at 10X (Olympus IX71, Tokyo, Japan) observation (Figure3.21).

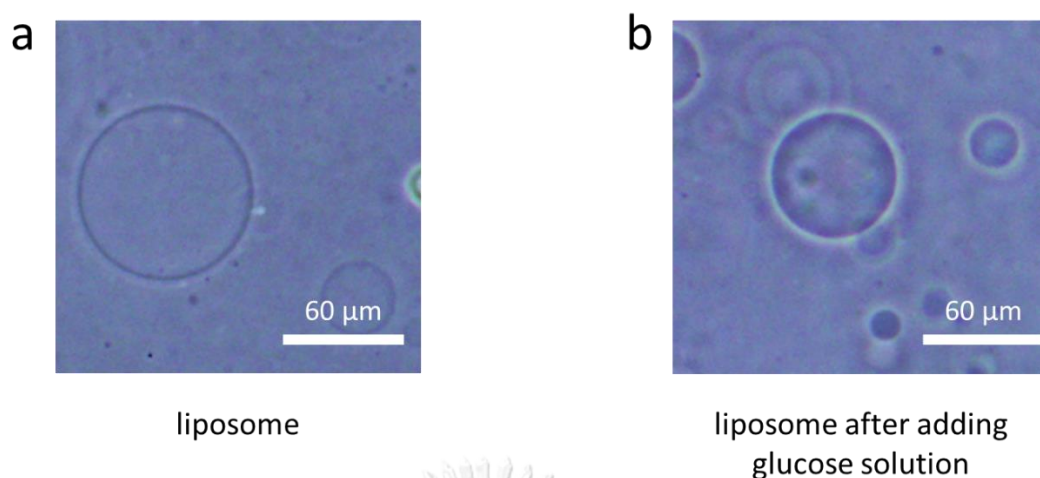


Figure 3. 21 The untreated liposome (a) and liposome after glucose adding (b)

Liposome in sucrose solution was prepared by electroformation (Figure 3.21, a). Under phase contrast mode, the same color between the inside and the outside of liposome was observed. After that, the glucose solution was added to the outside of liposome suspension. Under phase contrast mode, the different color between the inside and the outside of liposome was observed due to the difference in density of solution inside and outside of liposomes (Figure 3.21, b).

These differences will be disappeared when the liposome leaks. Then, introduce oxidized carbon particle into the prepared liposome suspension and observed the difference between the color of the inside and the color outside of liposome. Among the three sizes of oxidized carbon particle study 50, 140 and 700 nm, only 140 nm of oxidized carbon particle (OP3.1) could induce liposome leakage. In the presence of 50 nm oxidized carbon particles, the difference between the color of the inside and the color outside of liposome was preserved for all liposome even after being incubated with the particle for 240 min. In contrast, when the 140 nm of oxidized carbon particle were introduced into liposome suspension, the difference between the color of the inside and the color outside of liposome start to disappear after 60 min of incubation. As a result, we conduct

that oxidized carbon with the size of 140 nm can induce lipid bilayer membrane leakage, whereas the smaller size (50 nm) and the bigger size (700 nm) cannot (Figure 3.22). In this result agree with previous studies in which oxidized carbon particle of 130 nm prepared from oxidation/exploration of graphite [14-16] or from direct oxidation of carbon black [17] could effectively induce lipid bilayer membrane leakage.

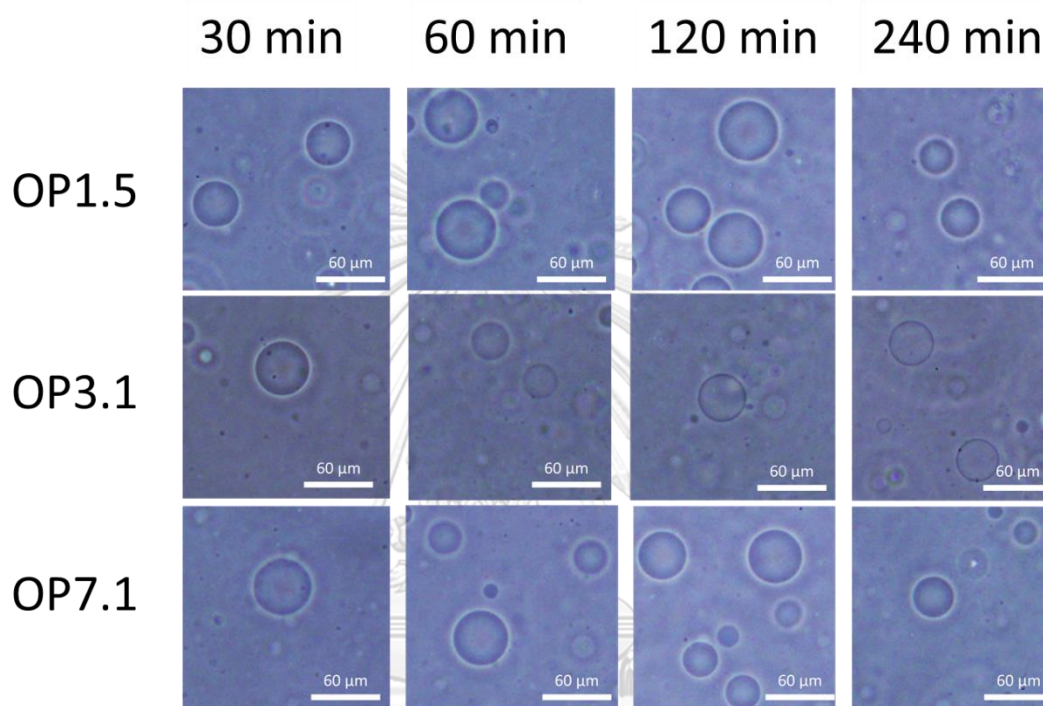


Figure 3. 22 Phase contrast image of liposome after being incubated with oxidized carbon particles for 30, 60, 120 and 240 min.

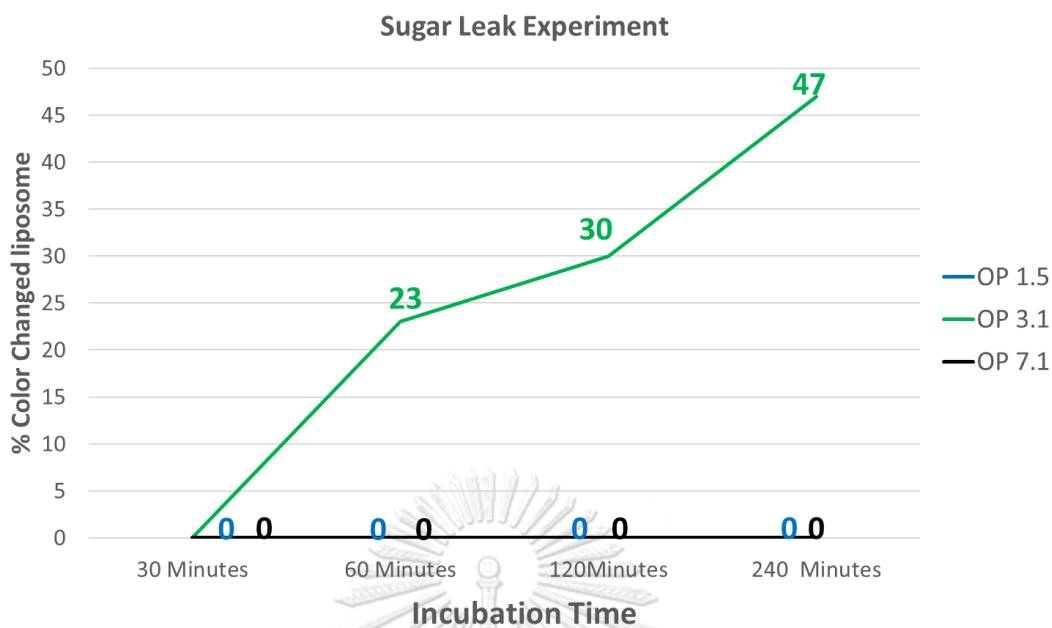


Figure 3. 23 The percentage of phase contrast changed of liposome after incubated with oxidized carbon particles for 30, 60, 120 and 240 min.

The number of liposome that their interior show similar color to the medium color, are counted as a function of incubation. The percentage of the same color between the inside and the outside of liposome are 0, 23, 30 and 47% due to are incubated with OP3.1 at 30, 60, 120 and 240 min, respectively as shown in **Figure 3.23**.

These results indicate that only OP3.1 could induce membrane leakage of the liposome. Thus, the solution between inside and outside could be exchanged until balance, probably through the transient pore formation on lipid bilayer membrane.

CHAPER IV CONCLUSION

Our objective here is to investigate the effect of the *size* of oxidized carbon particles on lipid bilayer membrane leak induction. Our challenge is the preparation of oxidized carbon of various sizes. We have successfully prepared three different sizes, 50, 140 and 700 nm, oxidized carbon particles by 4 steps process. Step1: polystyrene particle could be prepared via emulsion polymerization and their sizes could be controlled to adjusting the concentration of surfactant and monomer. Step 2: we successfully hypercrosslink the obtained PSs by Friedel Craft alkylation reaction. Step 3: we successfully prepared carbon particles by pyrolytic the hypercrosslink particles. Step 4: The water immiscible particles were oxidized into oxidized carbon particles. Through, the use of cell-sized liposome, we have demonstrated that the among 50, 140 and 700 nm oxidized carbon particle, only 140 nm oxidized carbon particle could induce lipid bilayer membrane leakage.

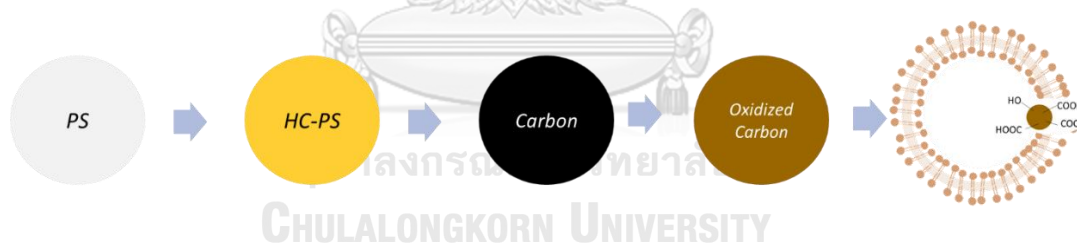


Figure 4. 1 Illusion for preparation of various sized of oxidized carbon nanosphere and study their ability to induce a leakage on lipid bilayer membrane

Table 4. 1 Summary of particle size in each step of oxidized carbon nanosphere preparation and their ability to induce a leakage on lipid bilayer membrane.

| Conditions | Size of PSs (nm) | Size of HC-PSs (nm.) | Size of CARBON (nm.) | Size of OPs (nm.) | Membrane leakage |
|------------|------------------|----------------------|----------------------|-------------------|------------------|
| 1 | 59±9.1 | 59±7.3 | 56±10 | 57±11 nm | ✗ |
| 2 | 147±16.7 | 158±14.3 | 140±17.8 | N/A | N/A |
| 3 | 200±20.0 | 176±15.2 | 156±12.4 | 137±9.49nm | ✓ |
| 4 | 273±26.0 | 240±16.1 | 246±16.2 | N/A | N/A |
| 5 | 415±24.7 | 635±55.1 | 538±32.0 | N/A | N/A |
| 6 | 643±39.8 | 639±171 | 556±44.3 | N/A | N/A |
| 7 | 811±91.0 | 831±137 | 820±49.7 | 716±113nm | ✗ |

REFERENCES

1. Lee, S. H.; Castagner, B.; Leroux, J. C., Is there a future for cell-penetrating peptides in oligonucleotide delivery? *Eur J Pharm Biopharm* **2013**, *85* (1), 5-11.
2. Wang, F.; Wang, Y.; Zhang, X.; Zhang, W.; Guo, S.; Jin, F., Recent progress of cell-penetrating peptides as new carriers for intracellular cargo delivery. *J Control Release* **2014**, *174*, 126-36.
3. Chen, L.; Fang, S.; Xiao, X.; Zheng, B.; Zhao, M., Single-Stranded DNA Assisted Cell Penetrating Peptide-DNA Conjugation Strategy for Intracellular Imaging of Nucleases. *Anal Chem* **2016**, *88* (23), 11306-11309.
4. Loney, C.; Vandenbranden, M.; Ruyschaert, J.-M., Cationic liposomal lipids: from gene carriers to cell signaling. *Progress in lipid research* **2008**, *47* (5), 340-347.
5. Gehl, J., Electroporation: theory and methods, perspectives for drug delivery, gene therapy and research. *Acta Physiologica Scandinavica* **2003**, *177* (4), 437-447.
6. Lakshmanan, S.; Gupta, G. K.; Avci, P.; Chandran, R.; Sadasivam, M.; Jorge, A. E.; Hamblin, M. R., Physical energy for drug delivery; poration, concentration and activation. *Adv Drug Deliv Rev* **2014**, *71*, 98-114.
7. Caban, S.; Aytakin, E.; Sahin, A.; Capan, Y., Nanosystems for drug delivery. *OA Drug Design & Delivery* **2014**, *18* (2), 1-7.
8. McMahon, H. T.; Boucrot, E., Molecular mechanism and physiological functions of clathrin-mediated endocytosis. *Nature reviews Molecular cell biology* **2011**, *12* (8), 517.
9. Sulheim, E. Mechanisms of Cellular Uptake and Intracellular Degradation of Polymeric Nanoparticles. Institutt for fysikk, 2014.
10. Tree-Udom, T.; Seemork, J.; Shigyou, K.; Hamada, T.; Sangphech, N.; Palaga, T.; Insin, N.; Pan-In, P.; Wanichwecharungruang, S., Shape Effect on Particle-Lipid Bilayer Membrane Association, Cellular Uptake, and Cytotoxicity. *ACS Appl Mater Interfaces* **2015**, *7* (43), 23993-4000.
11. Adjei, I. M.; Sharma, B.; Labhasetwar, V., Nanoparticles: cellular uptake and

cytotoxicity. *Adv Exp Med Biol* **2014**, *811*, 73-91.

12. Hühn, D.; Kantner, K.; Geidel, C.; Brandholt, S.; De Cock, I.; Soenen, S. J.; Rivera_Gil, P.; Montenegro, J.-M.; Braeckmans, K.; Mullen, K., Polymer-coated nanoparticles interacting with proteins and cells: focusing on the sign of the net charge. *ACS nano* **2013**, *7* (4), 3253-3263.
13. Hamada, T.; Morita, M.; Miyakawa, M.; Sugimoto, R.; Hatanaka, A.; Vestergaard, M. C.; Takagi, M., Size-dependent partitioning of nano/microparticles mediated by membrane lateral heterogeneity. *J Am Chem Soc* **2012**, *134* (34), 13990-6.
14. Arayachukeat, S.; Palaga, T.; Wanichwecharungruang, S. P., Clusters of carbon nanospheres derived from graphene oxide. *ACS Appl Mater Interfaces* **2012**, *4* (12), 6808-15.
15. Arayachukiat, S.; Seemork, J.; Pan-In, P.; Amornwachirabodee, K.; Sangphech, N.; Sansureerungsikul, T.; Sathornsantikun, K.; Vilaivan, C.; Shigyou, K.; Pienpinijtham, P.; Vilaivan, T.; Palaga, T.; Banlunara, W.; Hamada, T.; Wanichwecharungruang, S., Bringing macromolecules into cells and evading endosomes by oxidized carbon nanoparticles. *Nano Lett* **2015**, *15* (5), 3370-6.
16. Seemork, J.; Sansureerungsikul, T.; Sathornsantikun, K.; Sinthusake, T.; Shigyou, K.; Tree-Udom, T.; Jiangchareon, B.; Chiablaem, K.; Lirdprapamongkol, K.; Svasti, J.; Hamada, T.; Palaga, T.; Wanichwecharungruang, S., Penetration of Oxidized Carbon Nanospheres through Lipid Bilayer Membrane: Comparison to Graphene Oxide and Oxidized Carbon Nanotubes, and Effects of pH and Membrane Composition. *ACS Appl Mater Interfaces* **2016**, *8* (36), 23549-57.
17. Amornwachirabodee, K.; Tantimekin, N.; Pan-In, P.; Palaga, T.; Pienpinijtham, P.; Pipattanaboon, C.; Sukmanee, T.; Ritprajak, P.; Charoenpat, P.; Pitaksajjakul, P., Oxidized Carbon Black: Preparation, Characterization and Application in Antibody Delivery across Cell Membrane. *Scientific reports* **2018**, *8* (1), 2489.
18. Arnal, C.; Alzueta, M.; Millera, A.; Bilbao, R., Experimental And kinetic Study of the Interaction of a Commercial Soot Toward NO at High Temperature. *reactions* **2011**, *8*, 2.
19. Oh, W. K.; Yoon, H.; Jang, J., Size control of magnetic carbon nanoparticles for

drug delivery. *Biomaterials* **2010**, *31* (6), 1342-8.

20. Ouyang, Y.; Shi, H.; Fu, R.; Wu, D., Highly monodisperse microporous polymeric and carbonaceous nanospheres with multifunctional properties. *Sci Rep* **2013**, *3*, 1430.
21. Lee, W. H.; Moon, J. H., Monodispersed N-doped carbon nanospheres for supercapacitor application. *ACS Appl Mater Interfaces* **2014**, *6* (16), 13968-76.
22. Jinhua, L.; Guangyuan, Z., Polystyrene Microbeads by Dispersion Polymerization: Effect of Solvent on Particle Morphology. *International Journal of Polymer Science* **2014**, *2014*, 1-4.
23. Shim, S. E.; Cha, Y. J.; Byun, J. M.; Choe, S., Size control of polystyrene beads by multistage seeded emulsion polymerization. *Journal of Applied Polymer Science* **1999**, *71* (13), 2259-2269.
24. van Swaay, D.; deMello, A., Microfluidic methods for forming liposomes. *Lab Chip* **2013**, *13* (5), 752-67.
25. Patil, Y. P.; Jadhav, S., Novel methods for liposome preparation. *Chem Phys Lipids* **2014**, *177*, 8-18.
26. Lee, E. S.; Robinson, D.; Rognlien, J. L.; Harnett, C. K.; Simmons, B. A.; Ellis, C. B.; Davalos, R. V., Microfluidic electroporation of robust 10- μ m vesicles for manipulation of picoliter volumes. *Bioelectrochemistry* **2006**, *69* (1), 117-125.
27. Wu, H.-D.; Wu, S.-C.; Wu, I.-D.; Chang, F.-C., Novel determination of the crystallinity of syndiotactic polystyrene using FTIR spectrum. *Polymer* **2001**, *42* (10), 4719-4725.
28. Li, J.; Wang, X.; Zhang, T.; Wang, C.; Huang, Z.; Luo, X.; Deng, Y., A review on phospholipids and their main applications in drug delivery systems. *Asian journal of pharmaceutical sciences* **2015**, *10* (2), 81-98.



จุฬาลงกรณ์มหาวิทยาลัย
CHULALONGKORN UNIVERSITY

VITA

NAME Titiporn Sansureerungsikul

DATE OF BIRTH 02 May 1993

PLACE OF BIRTH Ratchaburi

INSTITUTIONS ATTENDED Bachelor's Degree of Science in Chemistry from Chulalongkorn University in 2012.

HOME ADDRESS

AWARD RECEIVED Third prize of best poster award from The 6 th Asian Symposium on Advanced Materials: Chemistry, Physics & Biomedicine of Functional and Novel Materials (ASAM-6)
รางวัลการเขียนข้อเสนอโครงการนวัตกรรมสายอุดมศึกษา ประจำปี 2559 รางวัลชนะเลิศ และรางวัลผลงานนวัตกรรมสายอุดมศึกษา ประจำปี 2559 รางวัลระดับดีมาก จากงานมหกรรมงานวิจัยแห่งชาติ 2559